Wave hindcast in the North Pacific area considering the propagation of surface disturbances

Yukiharu Hisaki

This is an Author's Accepted Manuscript of an article published in

Progress in Oceanography

Volume 165, July-August 2018, Pages 332-347.

Available online at: https://doi.org/10.1016/j.pocean.2018.06.003

Keywords: North Pacific Ocean; Interpolation; Wind; Cyclone; Wave model; Wave height; Wave period

Wave hindcast in the North Pacific area considering the propagation of surface disturbances

Yukiharu Hisaki[a,*]

[a] *University of the Ryukyus, 1-Aza Senbaru, Nishihara-cho, Okinawa, 903-0213 Japan. Tel. +81-98-895-8515; Fax: +81-98-895-8552*

Abstract

Ocean surface waves in the North Pacific area are affected by storm winds. It is necessary to consider the movement of storms to predict waves. The impact of a time interpolation method for winds that considers the propagation of surface disturbances on ocean wave prediction from 2005 to 2006 in the North Pacific area is demonstrated. It is possible to interpolate surface winds, even when there are multiple cyclones and anticyclones moving in different directions at different distances. This method will be useful for wind fields with increasing amounts of spatial information. The predicted wave heights and periods from the linearly interpolated winds and the winds predicted using this new method are compared with in-situ observations from several moored buoys. The predicted wave heights are also compared with those from several drifting buoys in the northwestern Pacific. The improvement of the wave height and period prediction is evident in the case where the difference in the predicted wave parameters between the linear interpolation and the present method is large. The improvement of the wave height and

*Corresponding author

Email address: `hisaki@sci.u-ryukyu.ac.jp` (Yukiharu Hisaki)

period prediction is statistically significant at more than 95 % in most cases. It is shown that the wave height and period prediction can be improved by improving the time interpolation method; however, the improvement of the wave direction prediction is not evident.

Keywords: North Pacific Ocean; Interpolation; Wind; Cyclone; Wave model; Wave height; Wave period.

---

1. Introduction

Knowledge of the wave climate is important for ocean wave research and for practical applications such as ship navigation, offshore oil exploration, and the planning of marine operations and offshore and coastal structures. Wave heights are high during the winter in the North Pacific area, including the Bering Sea and the Sea of Okhotsk. Extratropical cyclones often occur and develop in the North Pacific area. These extratropical cyclones cause extremely high waves. A hindcast of ocean waves is important for climate studies and for practical applications such as scheduling ship navigation and maintaining fisheries. The prediction and hindcast of ocean waves is often used (e.g., Chawla et al., 2013; Chowdhury and Behera, 2017; Cox and Swail, 2001; Reguero et al., 2012; Sasaki, 2014; Wang and Swail, 2001; Yamaguchi and Hatada, 2002) for wave climate studies. Ocean wave models for hindcasts are driven by archived atmospheric reanalysis datasets. However, the time resolution of archived atmospheric reanalysis data T is much longer than the time step required for wave prediction. Therefore, the surface wind is interpolated with respect to time.

It may be better to compute surface winds from atmospheric models incorporating observed data; however, this would result in a computational overload. A linear interpolation with respect to time is often used because it is simple and robust. However, a linear time interpolation cannot retrieve the atmospheric fields in the case of a moving cyclone. A moving tropical cyclone is expressed by a parametric form (e.g., Hisaki and Naruke, 2003; Hong and Yoon, 2003), and the surface wind field is deduced from the parametric model. A Rankine vortex is often used for the parametric model (e.g., Cheung et al., 2007; Phadke et al., 2003). This approach may be useful for case studies that investigate the ocean response to a moving storm. However, it is difficult to apply this method when both moving cyclones and stationary fields coexist. An interpolation using the parametric form is generally applied in the area near the moving cyclones for each cyclone, while linear interpolations are applied in other areas. The problem is how to decide which areas use the parametric interpolation and which areas use the linear interpolation.

It is also difficult to express moving extratropical cyclones using the parametric form, such as a Rankine eddy. Waves associated with extratropical cyclones are predicted not from the parametric form of the cyclone but from the interpolated wind of the gridded data (e.g., Businger et al., 2015; Pingree-Shippee et al., 2016). Cieślikiewicz and Graff (1997) reconstructed the wind fields using the empirical orthogonal function (EOF) method, in which the spatial patterns are fixed; however, a propagating pattern cannot be reconstructed using this method.

Hisaki (2016) developed a new and simple time interpolation method of an atmospheric field that can be applied to both moving and stationary disturbances. This method is called the Space Propagation Time Interpolation

Method (SPTIM). The principle of SPTIM is similar to the interpolation method in Hisaki (2011), which can remove the Garden Sprinkler effect by interpolating a wave directional spectrum at higher frequency and direction resolution from a wave spectrum at low spectral resolution. Hisaki (2016) demonstrated that the predicted near inertial currents using winds interpolated from SPTIM are significantly different from those from linearly interpolated winds, even though the wind products for the prediction are the same. This method becomes obsolete with increasing amounts of temporal wind field information. However, it is useful with increasing spatial wind field information because the grid number difference in the position of a cyclone at a time t with that at a time $t + T$ is larger with higher spatial resolution (Hisaki, 2016).

There are studies that have investigated the wave predictions from different wind products in the the global ocean (e.g., Campos and Soares, 2016; Caires et al., 2004; Graber et al., 1995; Stopa and Cheung, 2014). The wind products in these studies have different time and spatial resolutions. There are few studies that investigate the impact of the time interpolation method on wave predictions using the same wind data products. Van Vledder and Akpınar (2015) showed that a finer time resolution in the wind fields does not significantly improve the accuracy of the wave predictions.

The objective of the study is to demonstrate SPTIM for ocean surface wave prediction from 2005 to 2006 in the North Pacific area. The predicted wave parameters are compared with in-situ observed data obtained from deployed buoys. The positions of the deployed buoys are geographically limited to the North Pacific near the US coast.

A few moored buoy datasets in the northwestern Pacific were used in Cox and Swail (2001) and Yamaguchi and Hatada (2002). However, these moored buoys were dismantled in 2000. There were no moored buoys in the northwestern Pacific around Japan during the analysis period used in this study. Most validation studies of wave hindcasts have not been compared to in-situ observations in the northwestern Pacific (Caires et al., 2004; Reguero et al., 2012; Stopa and Cheung, 2014), and validation studies of wave predictions using buoy datasets in the northwestern Pacific are rare. Comparisons of predicted wave parameters with other instruments are limited to satellite altimeter data. The validation of satellite altimeter wave height data in the northwestern Pacific is limited. For example, Zieger et al. (2009) validated satellite altimeter wave height data via comparisons to buoy data; however, there are no buoy data in the northwestern Pacific.

We did comparisons with drifting buoy data in the northwestern Pacific. Studies that compare predicted wave parameters with drifting buoy data are rare (Doble and Bidlot, 2013; Waseda et al., 2014).

The difference between linearly interpolated winds and winds interpolated by SPTIM is large in the storm track area of the northwestern Pacific (Hisaki, 2016). The storm track area is observed along the major oceanic frontal zones in the northwestern Pacific (Nakamura et al., 2004). The wave data from drifting buoys are suitable for demonstrating the ability of SPTIM to predict wave parameters because many of the drifting buoys have moved to the Kuroshio extension area.

This paper is organized as follows. Section 2.1 briefly reviews SPTIM. Section 2.2 describes the wave modeling and observations. Section 3.1 shows an example of a wave prediction. The wind and wave parameters are compared with moored buoy observations in Sections 3.2, 3.3, and 3.4. The wave heights are compared with drifting buoy observations in Section 3.6. The wave directions are compared in Section 3.5. The spatial and temporal variability of the predicted wave parameters from the linear interpolation and SPTIM are investigated in Section 3.7. The discussion and conclusions are presented in Section 4.

2. Methods

2.1. Interpolation method

The details of the interpolation method are described in Hisaki (2016). The outline of the method is briefly described here. We consider the interpolation of a scalar value $P = P_1(\mathbf{x})$ at a position $\mathbf{x}$ and a time t and $P = P_2(\mathbf{x})$ at a position $\mathbf{x}$ and a time $t+T$. The value of P at the time $t+\alpha_t T$ $(0<\alpha_t< 1)$ is $P=(1-\alpha_t)P_1 + \alpha_t P_2$ in the case of linear interpolation. If we consider the movement of the disturbance, this is extended as

$$P(\mathbf{x} + \alpha_t \mathbf{a}) = (1-\alpha_t)P_1(\mathbf{x}) + \alpha_t P_2(\mathbf{x}_b), \tag{1}$$

where $\mathbf{x}_b = \mathbf{x}+\mathbf{a}$ and the vector $\mathbf{a} = \mathbf{a}(\mathbf{x})$ denotes the vector of the movement of the surface disturbance, which is called the propagation vector.

The propagation vectors $\mathbf{a}$ are estimated on all the grid points of the computational domain. We seek the centers of the surface disturbances at times t and $t+T$. The centers are those of the anticyclones or cyclones, which are identified as local maximum or minimum values of the sea level pressure.

The cyclones and anticyclones are tracked using the sea level pressure at the times t and $t + T$. The procedure for making pairs of (anti)cyclones is as follows. Consider that (anti)cyclones $C_t(i)$ $(i = 1, \ldots, M)$ and $C_{t+T}(j)$ $(j = 1, \ldots, N)$ are identified within the search window, where $C_t(i)$ denotes the (anti)cyclones at the time t and M and N are the number of (anti)cyclones at the times t and $t + T$, respectively. We seek $j_q(i) = j$ to minimize $|\mathrm{SLP}(C_t(i)) - \mathrm{SLP}(C_{t+T}(j))|$ for each i, where $\mathrm{SLP}(C_t(i))$ is the central sea level pressure of the (anti)cyclone $C_t(i)$.

If there exists no k for i $(i, k = 1, \ldots, M)$ that satisfies $j_q(i) = j_q(k)$ except $i \neq k$, a pair of (anti)cyclones $(C_t(i),C_{t+T}(j_q(i)))$ is identified. If there exists a k for i $(i, k = 1, \ldots, M)$ that satisfies $j_q(i) = j_q(k)$ and $i \neq k$, the distances $\mathrm{dist}(C_t(i), C_{t+T}(j_q(i)))$ and $\mathrm{dist}(C_t(k), C_{t+T}(j_q(k)))$ are compared, where $\mathrm{dist}(C_t(i), C_{t+T}(j))$ is the distance between the centers of the (anti)cyclones $C_t(i)$ and $C_{t+T}(j)$. If $\mathrm{dist}(C_t(i), C_{t+T}(j_q(i))) < \mathrm{dist}(C_t(k), C_{t+T}(j_q(k)))$, a pair of (anti)cyclones $(C_t(i),C_{t+T}(j_q(i)))$ is identified. The number of (anti)cyclone pairs cannot be larger than M or N. There exists the possibility that (anti)cyclone pairs are overlooked. This method should therefore be improved by incorporating the track method in Neu et al. (2013).

The positions of the centers of the disturbances are $\mathbf{x}_p(n)$ and $\mathbf{x}_q(n)$ $(n{=}1, \ldots, M_D)$ at times t and $t + T$, respectively, where M_D is the number of pairs of centers of anticyclones or cyclones. The positions $\mathbf{x}_p(n)$ and $\mathbf{x}_q(n)$ are considered to be the positions for the same anticyclones or cyclones. The propagation vectors $\mathbf{a}$ in Eq. (1) on $\mathbf{x}_p(n)$ $(n{=}1, \ldots, M_D)$ are $\mathbf{x}_q(n){-}\mathbf{x}_p(n)$.

The propagation vectors $\mathbf{a}$ on the other grid points are spatially interpolated from $\mathbf{a}$ at the positions $\mathbf{x}_p(n)$. If the area of the analysis is limited, the propagation vector $\mathbf{a}$ on the boundary is $\mathbf{0}$. Both position vectors $\mathbf{x}$ and $\mathbf{x}+\mathbf{a}$ are on grid points. In this case, the position $\mathbf{x}+\alpha_t\mathbf{a}$ in Eq. (1) is not on a grid point. Instead of the spatial interpolation of P evaluated in Eq. (1) at positions $\mathbf{x}+\alpha_t\mathbf{a}$ to the grid points, we estimate the position $\mathbf{x}_a$ by solving the equation

$$\mathbf{x}_c = \mathbf{x}_a + \alpha_t \mathbf{a}(\mathbf{x}_a) \qquad (2)$$

for a given grid position $\mathbf{x}_c$, where $\mathbf{a}(\mathbf{x}_a)$ is the bilinearly interpolated $\mathbf{a}$ from the propagation vectors $\mathbf{a}$ onto the grid points. The value of $P = P_1(\mathbf{x}_a)$ at the time t is evaluated using the bilinear interpolation from P_1 on the grid points. The value of $P = P_2(\mathbf{x}_a + \mathbf{a}(\mathbf{x}_a))$ at the time $t + T$ is evaluated using the bilinear interpolation from P_2 on the grid points. Then, the value of P at the time $t+\alpha_t T$ is evaluated using Eq. (1) by replacing $\mathbf{x}$ with $\mathbf{x}_a$. This interpolation is conducted in components for the wind vectors. In the case where the propagation vector $\mathbf{a}$ is $\mathbf{0}$, SPTIM is identical to the linear interpolation. An ad-hoc correction is conducted near the coast (Hisaki, 2016).

2.2. Model and data

The ECMWF ERA-Interim surface wind data and sea level pressure (http://apps.ecmwf.int/datasets/data/interim-full-daily/) were used to predict the wave spectra. The spatial resolution is $0.75° \times 0.75°$, and the time resolution is 6 hours.

The wave spectra $F = F(f, \theta, \mathbf{x}, t)$, where f is the wave frequency, θ is the wave direction, $\mathbf{x}$ is the position, and t is the time, are predicted using the energy balance equation for deep water. The parameterization of the source function S is the same as that of WAM (Wave Modeling) cycle-4 (e.g., WAMDI Group et al., 1988; Wise Group et al., 2007). The wind input source function is from Janssen (1991), the dissipation source function is from Komen et al. (1984), and the nonlinear interaction source function is from Hasselmann et al. (1985). The ratio of adjacent frequencies was 1.1, and the resolution of the wave direction was 15°. The frequency is from 3.505×10^{-2} Hz to 0.345 Hz. The spatial grid for the wave prediction is the same as that of the ECMWF Interim data and is 0.75° × 0.75°. The area of the computation is from 135° E to 150° W and from 20.25° N to 64.5° N. This computation area was selected to cover the NDBC (National Data Buoy Center) buoys and the storm track area in the northwestern Pacific and due to the computation limitations of the personal computer used. The wave spectra on the upwind boundary were evaluated by solving $\partial F/\partial t = S$.

The time step of the computation was 15 min. The wind data were interpolated for 15-min intervals between 7.5 min and 52.5 min of every hour. The wave spectra were computed from 0 min to 45 min of every hour. The wave parameters at every hour were compared to the in-situ observations.

The wave data of NDBC in Figure 1a was used for the comparison. The wind is observed 5 m above sea level, and the wind speed at a height of 10 m is estimated from the power law of the wind speed using the method of Hsu et al. (1994).

The wave heights $H_s = 4M_{0,0,0}^{1/2}$, periods $T = M_{0,0,0}M_{1,0,0}^{-1}$, and directions $\theta_v = \mathrm{Arg}(M_{0,1,0}, M_{0,0,1})$ are estimated from the wave spectrum $F(f,\theta)$, where

$$M_{p,q,r} = \int_0^\infty \int_{-\pi}^{\pi} f^p \cos^q \theta \sin^r \theta F(f,\theta) d\theta df \qquad (3)$$

and $\mathrm{Arg}(X,Y)$ denotes an argument of a complex number $X+iY$. The model predicted wave height, period, and direction from the linearly interpolated winds are referred to as H_{sL}, T_L, and θ_{vL}. The model predicted wave height, period, and direction from the winds interpolated by SPTIM are referred to as H_{sS}, T_S, and θ_{vS}. The buoy-observed wave height, period, and direction are referred to as H_{sB}, T_B, and θ_{vB}. The buoy-observed wind, the linearly interpolated wind from the ECMWF ERA-Interim surface wind data, and the wind interpolated by SPTIM are denoted as $\mathbf{U}_B$, $\mathbf{U}_L$, and $\mathbf{U}_S$, respectively. The wind speeds are $U_B = |\mathbf{U}_B|$, $U_L = |\mathbf{U}_L|$, and $U_S = |\mathbf{U}_S|$.

The hourly data were analyzed, and the period of the analysis was from January 1, 2005, to December 31, 2006. The locations of the NDBC buoys are indicated in Figure 1a. Table 1 summarizes the NDBC buoy specifications. The wave data from these buoys are collected at least more than one year. The number of wave data N_{wn} is different from the number of wind data N_{wn} because the wind and wave sensors are different. The wave directions were only observed at buoy U (51001) during the analysis period. We can download the data of $P(f)$ and $\theta_v(f)$, where $P(f)$ is a frequency spectrum and $\theta_v(f)$ is the spectral mean wave direction at a frequency f. The mean wave directions are evaluated as

$$\theta_{vB} = \mathrm{Arg}(\int_0^{f_u} \cos\theta_v(f)P(f)df, \int_0^{f_u} \sin\theta_v(f)P(f)df), \quad (4)$$

where $f_u = 0.485$ Hz is the upper frequency.

We also compared the predicted wave heights with data observed by a drifting JMA (Japan Meteorological Agency) buoy. The drifting JMA buoy data are available at http://www.data.jma.go.jp/gmd/kaiyou/db/vessel_obs/data-report/html/buoy/buoy_e.php. The wave height is observed by the drifting buoy at 3-hour intervals. The resolution of the wave height is 0.1 m.

Figure 1b shows the trajectory of the drifting JMA buoys. The analysis period and the number of data points of the JMA drifting buoys are summarized in Table 2. The area for the comparison is north of 30° N and east of 145° E to avoid the areas close to land and to the boundary of the computational area. Seven drifting buoys were used for the comparison and are labeled A–G in Figure 1b and Table 2. The number of total comparisons is $N_{wv} = 3955$, which is much smaller than that with the NDBC buoys. Most of the JMA drifting buoys are drifting in the Kuroshio extension current.

3. Results

3.1. Example of a wave prediction

Figure 2 shows examples of interpolations of the wind. Figure 2a shows time series of the wind speeds at the NDBC Buoy P (46071) location (51.141° N, 179.119° W) from 0 UTC to 12 UTC on August 25, 2005. The buoy-observed wind speeds increased until 2 UTC and then decreased (Figure 2a). The wind speeds from the SPT (Space Propagation Time)-interpolated wind vectors also increased until 2 UTC and then decreased. However, the temporary change in the buoy-observed wind speeds cannot be seen in the wind speeds from the linear interpolation. An artifact similar to a 6-hour-period spurious oscillation can be seen in the linearly interpolated wind speeds (Figure 2a).

Figures 2b and 2c show the wind vectors and wind speeds at 0 UTC and 6 UTC, respectively, on August 25, 2005. An extratropical cyclone with a center of (54.75° N, 177.75° E) can be seen at 0 UTC (Figure 2b). The buoy location is close to the maximum position of the wind speeds associated with the cyclone, which are located southeast of the cyclone center. The center of the cyclone is at (55.5° N, 177.75° W) at 6 UTC (Figure 2c), and the cyclone was moving northeastward at the time.

Figures 2d and 2e show the wind vectors and wind speeds estimated from the linear interpolation and SPTIM, respectively, at 4 UTC on August 25, 2005. The buoy location (the triangle in Figure 2b–f) is close to the maximum position of the wind speeds associated with the cyclone (Figure 2e), while the maximum position of the wind speeds in Figure 2d is not as close to the buoy position as those in Figures 2b and 2e. The wind speed maximum area in Figure 2d appears to be smeared. Figure 2f shows the differences in the wind vectors estimated from SPTIM and those estimated from the linear interpolation ($\mathbf{U}_S - \mathbf{U}_L$) and the differences in the wind speeds ($U_S - U_L$). A local maximum area with a large difference between U_S and U_L can be seen near (55° N, 180° E) in Figure 2f. The local maximum of $U_S - U_L$ at (54.75 N, 179.25° E) in Figure 2f is close to the local minimum position of the wind speeds at 00 UTC on August 25 (Figure 2b). We can see another local maximum of $U_S - U_L$ and a local minimum near the area that is close to the position of the local minimum wind speeds at 06 UTC on August 25. There is another cyclone around (43.5° N, 160° E) in Figure 2. The positions at which the differences between U_S and U_L are large are also close to the center of this cyclone.

Figure 3a shows time series of the wave heights (H_{sB}, H_{sL}, and H_{sS}) at the NDBC buoy location from 0 UTC to 12 UTC on August 25, 2005. The observed wave heights H_{sB} (blue) are the highest and the predicted wave heights from the SPTIM winds are the second highest throughout most of the period, while the buoy-observed wind speeds are lowest after 6 UTC in

Figure 2a. The wind speed differences $|U_L - U_B|$ are smaller than $|U_S - U_B|$ from 5 UTC to 11 UTC in Figure 2a. However, the wave height differences $|H_{sS} - H_{sB}|$ are smaller than $|H_{sL} - H_{sB}|$ in Figure 3a, which suggests that the estimation of the winds in the area surrounding the buoy location is greatly improved by SPTIM.

Figures 3b and 3c show the predicted wave heights from the linearly interpolated winds (H_{sL}) and those from the SPT-interpolated winds (H_{sS}) at 4 UTC on August 25, 2005. A local maximum of the wave heights associated with the cyclone can be seen at (51° N, 179.25 W), which is close to the position of the NDBC buoy (P) both in Figure 3b and in Figure 3c. The difference in the wave heights ($H_{sS} - H_{sL}$) is shown in Figure 3d. The local maximum position of the difference near the NDBC buoy position is at (54° N, 179.25 W), which is different from the maximum position of the wave heights. The difference in the wave heights ($H_{sS} - H_{sL}$) is positive around the area of the cyclone near the NDBC buoy, while there is an area where the value of $U_S - U_L$ is negative around (56° N, 180° E) in Figure 2f), which shows that the the wave height in the area is affected by the swell.

3.2. Comparisons of wave parameters with the total NDBC buoys

Figure 4a shows a comparison between the linearly interpolated wind speeds (U_L) and the six NDBC buoy-observed wind speeds (U_B). The number of total wind comparisons is $N_{wn} = 76,940$. The mean values of U_B and U_L are $\overline{U_B} = 8.906$ ms^{-1} and $\overline{U_L} = 8.121$ ms^{-1}, respectively. The RMSD (root-mean-square deviation) of the wind speeds is $R_d(U_B, U_L) = 1.905$ ms^{-1}, where $R_d(X, Y) = [\overline{(X - Y)^2}]^{1/2}$ denotes the RMSD between the parameters X and Y and $\overline{X}$ denotes the averaging of X. The correlation coefficient

$r_c(U_B, U_L)$ between the buoy-observed winds and the linearly interpolated winds is 0.913, where $r_c(X, Y)$ denotes the Pearson correlation between the parameters X and Y. The scatter plots indicate the percentage of the number of dots to the total number of dots in the 0.2 ms^{-1} bins. For example, the number of data points (U_L,U_B) satisfying $7.2 \leq U_L < 7.4$ ms^{-1} and $8.6 \leq U_B < 8.8$ ms^{-1} is 128, and the percentage of the data is $128/76,940 \simeq 0.166$ %, which is indicated by the red area in Figure 4a.

Figure 4c shows a comparison between the model-predicted wave heights from the linearly interpolated winds (H_{sL}) and the NDBC-buoy-observed wave heights (H_{sB}). The number of comparisons of wave heights is $N_{wv}= 89,318$, the RMSD of the wave heights is $R_d(H_{sB}, H_{sL})= 0.638$ m, and the correlation coefficient is $r_c(H_{sB}, H_{sL})= 0.893$. The correlation coefficients of both the wave height ($r_c(H_{sB}, H_{sL})$) and the wind speeds ($r_c(U_B, U_L)$) are approximately 0.9, and the model prediction is reasonable. The RMSD of the wave height is $R_d(H_{sB}, H_{sS})= 0.631$ m, and the correlation coefficient between the buoy wave heights and the SPTIM wave heights is $r_c(H_{sB}, H_{sS})$ =0.895, which is slightly lower and slightly higher than $R_d(H_{sB}, H_{sL})$ and $r_c(H_{sB}, H_{sL})$, respectively, but nearly the same.

Figure 4e shows a comparison of the observed wave periods (T_B) and the predicted wave periods from the linearly interpolated winds (T_L). Figure 4e shows the percentage of the data plotted in the 0.2-s bins. The RMSD of the wave periods is $R_d(T_B, T_L) = 1.312$ s, and the correlation is $r_c(T_B, T_L)= 0.747$ for $N_{wv}= 89,318$ data points. The RMSD and the correlation of the periods from the winds calculated by SPTIM are $R_d(T_B, T_S)= 1.301$ s and $r_c(T_B, T_S)$ = 0.749 s, respectively. They are also slightly smaller and slightly higher than $R_d(T_B, T_L)$ and $r_c(T_B, T_L)$, respectively.

Even though the prediction of the wind speeds, wave heights, and wave periods are improved by SPTIM, the improvement is very small over all. We selected the data for comparison as the absolute difference of the parameters from the linear interpolation and SPTIM is larger than a threshold. Figure 4b shows a scatter plot of the wind speeds (U_S-U_B and U_L-U_B) for $|U_S - U_L| > U_D$, and $U_D = 1.6$ ms^{-1}. Figure 4b shows a comparison of the wind speeds estimated from SPTIM and the linear interpolation only in the case where the difference in the model wind speeds is larger than 1.6 ms^{-1}. The value of $U_D = 1.6$ ms^{-1} is one example, and the dependency of the wind speed accuracy on U_D will be discussed.

The number of comparisons is N_{wn}= 337, which is $337/76,940 \simeq 0.438$ % of the total data. The mean buoy-observed, linearly interpolated, and SPT-interpolated wind speeds are $\overline{U_B} = 14.412$ ms^{-1}, $\overline{U_L} = 11.511$ ms^{-1}, and $\overline{U_S}$ = 12.789 ms^{-1}, respectively. The RMSD between U_B and U_L for $|U_S - U_L| > 1.6$ ms^{-1} is $R_d(U_B, U_L)$=5.138 ms^{-1}, and the correlation coefficient is $r_c(U_B, U_L)$=0.687. The RMSD between U_B and U_S for $|U_S - U_L| > 1.6$ ms^{-1} is $R_d(U_B, U_S)$=4.151 ms^{-1}, and the correlation coefficient is $r_c(U_B, U_S)$=0.737. Even though the wind speed estimation for $|U_S - U_L| > 1.6$ ms^{-1} is poorer than that of the total, the RMSD difference $R_d(U_B, U_L) - R_d(U_B, U_S)$ for this case is larger than $R_d(U_B, U_L) - R_d(U_B, U_S)$ of the total. The correlation difference $r_c(U_B, U_S) - r_c(U_B, U_L)$ in the case of $|U_S - U_L| > 1.6$ ms^{-1} is also larger that of the total. The difference in the RMSD is approximately 1 ms^{-1}, and $(R_d(U_B, U_L) - R_d(U_B, U_S)) / R_d(U_B, U_L) \simeq 0.238$, which corresponds to an approximate 24 % reduction in the RMSD from the linear interpolation in the case of $|U_S - U_L| > 1.6$ ms^{-1}.

Figure 4d shows a scatter plot of the wave heights (H_{sS}-H_{sB} and H_{sL}-H_{sB}) for $|H_{sL} - H_{sS}|> H_D$ and H_D= 0.3 m. The number of comparisons is N_{wv}= 462, which is $462/89,318 \simeq$0.517 % of the total data. The mean values of the wave heights are $\overline{H_{sB}} = 5.831$ m, $\overline{H_{sL}} = 5.269$ m, and $\overline{H_{sS}}$= 5.606 m, respectively, in this case. The RMSD between H_{sS} and H_{sB} is $R_d(H_{sB}, H_{sS})$ = 1.277 m, and the RMSD between H_{sL} and H_{sB} is $R_d(H_{sB}, H_{sL}) = 1.456$ m. The correlation between H_{sS} and H_{sB} is $r_c(H_{sB}, H_{sL}) = 0.789$, while the correlation between H_{sS} and H_{sB} is $r_c(H_{sB}, H_{sS}) = 0.819$.

Figure 4e shows a scatter plot of the wave periods (T_S-T_B and T_L-H_B) for $|T_S - T_{sL}|$>T_D and $T_D = 0.2$ s. The number of comparisons is N_{wv}= 616, which is $616/89,318 \simeq$0.690 % of the total data. The mean values of the wave heights are $\overline{T_B} = 8.008$ s, $\overline{T_L} = 6.876$ s, and $\overline{T_S} = 6.997$ s, respectively, in Figure 4e. The RMSDs are $R_d(T_B, T_S) = 1.813$ s and $R_d(T_B, T_L) = 1.923$ s. The correlations are $r_c(T_B, T_L) = 0.712$ and $r_c(T_B, T_S) = 0.744$.

Figure 5 shows the RMSD and correlation coefficients as a function of the difference in the wind or wave parameters estimated from the linearly interpolated winds and the SPT-interpolated winds. The percentage of the data is also plotted as a function of the difference in Figure 5. The values of $R_d(U_B, U_L)$, $R_d(U_B, U_S)$, $r_c(U_B, U_L)$, and $r_c(U_B, U_S)$ in the case of $|U_S - U_L| > U_D$ are plotted against U_D in Figure 5a. The values of the RMSDs $R_d(U_B, U_L)$ and $R_d(U_B, U_S)$ increase with larger U_D. The difference $R_d(U_B, U_L)$ $-R_d(U_B, U_S)$ also increases with larger U_D. The correlations $r_c(U_B, U_L)$ and $r_c(U_B, U_S)$ decrease with higher U_D. The difference in the correlations can be seen from U_D=0.4 ms^{-1} in Figure 5a. The correlations for U_D=0.4 ms^{-1} are $r_c(U_B, U_L) = 0.850$ and $r_c(U_B, U_S) = 0.860$, respectively, and the number of data points is 4224 (5.490 % as in Figure 5b). The correlation $r_c(U_B, U_S)$ is higher than the correlation $r_c(U_B, U_L)$. The difference between the correlations ($r_c(U_B, U_S) - r_c(U_B, U_L)$) increases with larger U_D.

Figure 5c shows the RMDSs and correlations of the wave heights as a function of H_D in the case of $|H_{sS} - H_{sL}| > H_D$. The tendencies of the RMSDs and correlations in Figure 5c are similar to those in Figure 5a. The RMSDs $R_d(H_{sB}, H_{sL})$ (the red line in Figure 5c) and $R_d(H_{sB}, H_{sS})$ (the black line in Figure 5c) increase with higher H_D. The correlations $r_c(H_{sB}, H_{sL})$ (the blue line in Figure 5c) and $r_c(H_{sB}, H_{sS})$ (the green line in Figure 5c) decrease with higher H_D. The differences $R_d(H_{sB}, H_{sL}) - R_d(H_{sB}, H_{sS})$ and $r_c(H_{sB}, H_{sS}) - r_c(H_{sB}, H_{sL})$ increase with higher H_D. This shows that the efficacy of SPTIM compared to the linear interpolation is higher for larger differences between the predicted wave heights from the linearly interpolated winds (H_{sL}) and those predicted from the SPT-interpolated winds (H_{sS}).

Figure 5e shows the RMSDs and correlations of the wave periods as a function of T_D in the case of $|T_S - T_L| > T_D$. The tendencies of the RMSDs and correlations in Figure 5e are also similar to those in Figures 5a and 5c, even though there are some differences. The RMSDs $R_d(T_B, T_L)$ and $R_d(T_B, T_S)$ increase by $T_D \simeq 0.2$ s. The correlation $r_c(T_B, T_S)$ does not decrease with larger T_D. The difference in the correlations $r_c(T_B, T_S) - r_c(T_B, T_L)$ is evident with larger T_D.

The RMDSs between the predicted and observed wave parameters are larger for larger differences between the predicted wave parameters from the linearly interpolated winds and those from the SPT-interpolated winds. The predicted and observed wave parameters are more scattered and the bias between the predicted and observed wave parameters are larger for larger differences between the predicted wave parameters from the linearly interpolated winds and those from the SPT-interpolated winds.

Figures 5b, 5d, and 5f show the percentages of the number of data points satisfying $|U_S - U_L| > U_D$, $|H_{sS} - H_{sL}| > H_D$, and $|T_S - T_L| > T_D$, respectively. As explained in Figures 4b, 4d, and 4f, the values of the percentages are 0.438 %, 0.504 %, and 0.610 % for U_D= 1.6 ms^{-1}, H_D= 0.3 m, and T_D= 0.2 s, respectively. The curves in Figures 5b, 5d, and 5f are monotonically decreasing and are concave upward even in the linear-log plots. This shows that the numbers decrease rapidly as U_D (or H_D or T_D) increase from 0 and that the reduction rates of the numbers decrease with larger U_D (or H_D or T_D). The percentages are approximately 10 % at U_D $\simeq$0.26 ms^{-1}, H_D $\simeq$0.055 m, and T_D $\simeq$0.066 s in Figures 5b, 5d, and 5f, respectively. The improvements in the RMSDs and correlations (Figures 5a, 5c, and 5e) are small at these values of U_D, H_D, and T_D. We can see improvements at the values of U_D, H_D, and T_D where the percentages are on the order of 1 %. For example, the percentage for T_D =0.15 s is 1.664 % in Figure 5f, where an improvement in the correlation can be seen in Figure 5e.

3.3. Comparisons with each NDBC buoy

Tables 3 and 4 show comparisons of the predicted wind and wave parameters with the wind and wave parameters recorded by the NDBC buoys. The correlation of the wave height is greater than 0.9 for three of the buoys. The correlation of the wind speeds $r_c(U_B, U_L)$ is related to the correlation of the wave height $r_c(H_{sB}, H_{sL})$. For example, the correlation $r_c(U_B, U_L)$ at buoy R is the highest of all six buoys and the correlation $r_c(H_{sB}, H_{sL})$ at buoy T is the highest. The correlations $r_c(U_B, U_L)$ and $r_c(H_{sB}, H_{sL})$ at buoy U are the lowest of all six buoys. The order of the correlations $r_c(U_B, U_L)$ from high to low is R, T, S, Q, P, and U. The order of the correlations $r_c(H_{sB}, H_{sL})$ from high to low is T, R, Q, S, P, and U. The order of the correlations $r_c(T_B, T_L)$ from high to low is U, Q, T, R, S, and P. The correlations of the wave period $r_c(T_B, T_L)$ are not highly related to the correlations of the wind speeds $r_c(U_B, U_L)$. The prediction of the wave height is affected by the local winds, and the impact of the swell on the wave period prediction is larger than that on the wave height prediction. The correlations of the wind and wave parameters from the SPT-interpolated winds with the buoy-observed wind and wave parameters are higher than those from the linearly interpolated winds for all the buoys. The RMSDs of the wind and wave parameters from the SPT-interpolated winds with the buoy-observed wind and wave parameters are smaller than those from the linearly interpolated winds for almost all the buoys.

Figure 6 shows the accuracies of the wind and wave predictions versus the differences of these parameters, as in Figure 5, for each NDBC buoy. The RMSDs and correlations are plotted as a function of the differences between the linearly and SPT-interpolated parameters for each buoy. If the number of data points is small, the plots are not indicated. The numbers of wind and wave parameter data decrease rapidly with larger U_D, H_D, and T_D at buoy U. The difference between the linearly interpolated winds and the SPT-interpolated winds is small at lower latitudes because the number of moving storms is small in this area. The wave period is underestimated at buoy U because the swells from the west and south are not incorporated into the wave prediction.

There is nearly the same tendency at all of the buoys. The RMSDs increase with larger differences in the parameters (U_D, H_{sD}, and T_D). The dashed lines are above the solid lines in Figures 6a, 6c, and 6e, which indicates that the RMSDs for the SPT-interpolated parameters are smaller than those for the linearly interpolated parameters (i.e., $R_d(U_B, U_L) > R_d(U_B, U_S)$, $R_d(H_B, H_L) > R_d(U_B, U_S)$, and $R_d(T_B, T_L) > R_d(T_B, T_S)$) for all buoys. The differences of the RMSDs are larger with larger differences in the estimated parameters (U_D, H_{sD}, and T_D).

The correlations decrease with larger differences in the parameters. The solid lines are above the dashed lines in Figures 6b, 6d, and 6f for most of the buoys. This indicates that the correlations of the SPT-interpolated parameters are higher than those of the linearly interpolated parameters. There are some exceptions to these tendencies. For example, the correlations of the wind speeds with the linearly interpolated wind speeds are slightly larger than those with the SPT-interpolated wind speeds ($r_c(U_B, U_L) > r_c(U_B, U_S)$) at the NDBC buoy R (46073) (the green lines in Figure 6b). The correlations of the wind speeds at buoy R are higher than those at other buoys. The RMSDs $R_d(U_B, U_S)$ at buoy R are significantly smaller than the RMSDs $R_d(U_B, U_L)$. The total wind speed interpolation is therefore improved even at buoy R.

3.4. Statistical significance

The significance level of the improvement in the wave prediction in Figure 5 was investigated. The significance level is evaluated using the bootstrap method (e.g., Emery and Thomson, 1998). For a given U_D (or H_D or T_D), the effective sample size $N_e = N_e(k)$ ($N_e \leq N_c$) is evaluated for each buoy (e.g., Emery and Thomson, 1998; Trenberth, 1984), where $N_c = N_c(k)$ is the number of comparisons for each buoy and $k = 1, \ldots, 6$ is the buoy number, and they are N_{wn} or N_{wv}. The N_c data are treated as serial data, which underestimates the effective sample size N_e. $N_e = N_e(k)$ for each buoy data are resampled from $N_c = N_c(k)$ data using the bootstrap method. The correlation coefficients and RMSDs of the wave parameters are evaluated from $\sum_{k=1}^{6} N_e(k)$ data points. This calculation is repeated 10^4 times. The numbers of bootstraps in which the correlation coefficients increase and the RMSDs decrease using SPTIM are counted, and the significance levels are evaluated.

Figure 7 shows the significance level as a function of U_D, H_D, and T_D for Figure 5. For example, the significance levels at H_D= 0.1 m in Figure 7b are 99.6 % for the correlation (the red line) and 100 % for the RMSD (the blue line). The possibility that correlations between H_{sS} and H_{sB} are higher than those between H_{sL} and H_{sB} is 99.6 % in the case of $|H_{sS} - H_{sL}|$>0.1 m. The possibility of $R_d(H_{sB}, H_{sS}) < R_d(H_{sB}, H_{sL})$ is 100 % in the case of $|H_{sS} - H_{sL}|$>0.1 m. The significance level of $r_c(U_B, U_S) > r_c(U_B, U_L)$ is not as high (Figure 7a, red line), as the correlation coefficients $r_c(U_B, U_S)$ and $r_c(U_B, U_L)$, which are nearly the same as each other for smaller U_D (Figure 5a). However, they are more than 90 % in most of the cases in Figure 7a. The significance levels for the wave height and period predictions are not high for $H_D{\simeq}0$ and $T_D{\simeq}0$, respectively. The significance level of the improvement in the wave height is more than 95%, except for $H_D{\simeq}0$ m (Figure 7b). The correlations $r_c(T_B, T_S)$ and $r_c(T_B, T_L)$ are nearly the same, and the significance level of the improvement in the wave period correlation is not as high for $T_D{\simeq}0$. However, most of the significance levels for the wave height and period prediction improvements are greater than 95 %, except in these cases. The improvement in the wave prediction when using SPTIM is statistically significant over all.

In addition, we evaluated the significance levels of the wave prediction improvement for each buoy. However, the improvement was not very significant for some of the buoys because the number of comparisons was insufficient.

3.5. Comparison of wave directions

Figure 8 shows a comparison of the wave directions at buoy U. Figure 8a is a scatter density plot between the wave directions from the linearly interpolated winds ($\theta_v = \theta_{vL}$) and those observed by buoy U ($\theta_v = \theta_{vB}$) in $5^\circ{\times}5^\circ$ bins. The wave directions in Figure 8a indicate the direction from which the waves are coming and increase in the clockwise direction. The value of $\theta_v{=}0^\circ$ is from the north, and the value of $\theta_v{=}90^\circ$ is from the east. The density is the largest in the $80^\circ \leq \theta_{vL} < 85^\circ$ and $90^\circ \leq \theta_{vB} < 95^\circ$ bins, which are associated with easterlies. The RMSD between θ_{vL} and θ_{vB} is $R_d(\theta_{vL}, \theta_{vB}) = 33.86^\circ$, which is not very small. The RMSD between the linearly interpolated wind directions and the buoy-observed wind directions is 29.45°, which is comparable to $R_d(\theta_{vL}, \theta_{vB})$. In addition, swells from the west or south are not incorporated when predicting the wave spectrum around the area of buoy U. The RMSD between the wave directions from the SPTIM interpolated winds

(θ_{vS}) and the buoy-observed wave directions is $R_d(\theta_{vS}, \theta_{vB}) = 34.06°$, which is slightly larger than $R_d(\theta_{vL}, \theta_{vB})$.

Figure 8b shows $R_d(\theta_{vL}, \theta_{vB})$ and $R_d(\theta_{vS}, \theta_{vB})$ versus θ_D, which satisfies $|\theta_{vS} - \theta_{vL}| > \theta_D$. The RMSDs $R_d(\theta_{vL}, \theta_{vB})$ and $R_d(\theta_{vS}, \theta_{vB})$ are larger with larger θ_D for $\theta_D \simeq 12°$. However, the values of $R_d(\theta_{vS}, \theta_{vB})$ are larger than $R_d(\theta_{vL}, \theta_{vB})$ for larger θ_D. Figure 8c shows the ratio of the number of data points versus θ_D to the total number of data points (13, 726). The number of data points for larger θ_D is small. For example, the number of data points is only 62 and 0.452 % (62/13, 726) for $\theta_D = 12°$. Figure 8d shows the probability that $R_d(\theta_{vS}, \theta_{vB})$ is larger than $R_d(\theta_{vL}, \theta_{vB})$, as explained in Section 3.4. The number of data points for larger θ_D is small and the probability is at most 80 %. The prediction of the wave direction is not improved by SPTIM.

3.6. Comparison with JMA drifting buoys

Figure 9 shows a comparison of the wave heights from the JMA drifting buoys. Figure 9a shows a scatter plot between the predicted wave heights from the linearly interpolated winds (H_{sL}) and the JMA-buoy-observed wave heights (H_{sB}). The correlation coefficient is $r_c(H_{sB}, H_{sL}) = 0.856$, and the RMSD is $R_d(H_{sB}, H_{sL}) = 0.650$ m. The correlations and the RMSD are smaller than those of the NDBC buoys. The mean predicted and JMA-observed wave heights are $\overline{H_{sL}}= 2.174$ m and $\overline{H_{sB}}= 2.369$ m, respectively. These values are smaller than the NDBC buoy wave heights. The correlation between the predicted wave heights from the SPT-interpolated winds (H_{sS}) and the JMA-buoy-observed wave heights (H_{sB}) is $r_c(H_{sB}, H_{sS}) = 0.860$, which is slightly higher than $r_c(H_{sB}, H_{sL})$. The RMSD is $R_d(H_{sB}, H_{sS}) =$

0.641 m, which is slightly smaller than $R_d(H_{sB}, H_{sL})$. The mean model predicted wave height is $\overline{H_{sS}}$= 2.186 m.

Figure 9b shows the RMSD and the correlation coefficient versus H_D, which satisfies $|H_{sS} - H_{sL}| > H_D$. The general tendencies of the correlations and RMSDs are similar to those in Figure 5c. The correlations are smaller with larger H_D. The RMSDs are larger with larger H_D. The differences between the correlations ($r_c(H_{sB}, H_{sS})$ $-r_c(H_{sB}, H_{sL})$) are larger with increasing H_D. The differences between the RMSDs ($R_d(H_{sB}, H_{sL})$ $-R_d(H_{sB}, H_{sS})$) are also larger with increasing H_D.

Figure 9c shows the significance level versus H_D for Figure 9b as in Figure 7b. The method for the calculation is the same as that for Figure 7b. The effective sample size $N_e = N_e(k)$ (k=1, . . . , 7). $N_e(k)$ wave data points (H_{sB}, H_{sB}, H_{sL}) are resampled for each buoy number k (k=1, . . . , 7). The correlations ($r_c(H_{sB}, H_{sL})$ and $r_c(H_{sB}, H_{sS})$) and the RMSDs ($R_d(H_{sB}, H_{sL})$ and $R_d(H_{sB}, H_{sS})$) are estimated from the resampled wave data, and the improvement is evaluated. The possibility of an improvement is more than 90 % for 0.05 m$<H_D<$0.2 m.

The probability of $r_c(H_{sB}, H_{sS})>$ $r_c(H_{sB}, H_{sL})$ is low for $H_D \geq$0.2 m. This is due to the resampling in the bootstrap method. The correlation $r_c(H_{sB}, H_{sS})$ is smaller than $r_c(H_{sB}, H_{sL})$ in one of the buoys (buoy D). If $[\sum_{k=1}^{7} N_e(k)]$ data are resampled from the total buoy data, the probability of $r_c(H_{sB}, H_{sS})>$ $r_c(H_{sB}, H_{sL})$ is higher even for $H_D \geq$0.2 m. This problem can be resolved by increasing the amount of buoy data for the comparison.

Figure 9d shows the percentage of the wave data versus the difference H_D, as in Figure 5d. The number of wave data decreases significantly with larger

H_D. However, the decrease in the number of wave data is not as significant as in the case of the NDBC deployed buoy wave height data (Figure 5d). For example, the percentage in Figure 9d is 1.264 % for $H_D = 0.3$ m, while the percentage is 0.517 % in Figure 5d. The case where H_{sS} is different from H_{sL} at the JMA drifting buoy locations is more frequent than the case where H_{sS} is different from H_{sL} at the NDBC buoy locations, even though the mean value of the observed wave height $\overline{H_{sB}}$ by the NDBC buoys is larger than that observed by the JMA buoys. This is because the JMA drifting buoys are located in an area where storm tracks occur more frequently compared to the area where the NDBC buoys are located. An extratropical cyclone in the storm track area moves quickly due to the westerlies . Conversely, an extratropical cyclone north of the storm track area does not move as quickly; further, the winter cyclone frequency is higher in this area (e.g., Zolina and Gulev, 2002). Therefore, wave heights north of the storm track area are higher than those in the storm track area.

3.7. Spatial and temporal variability of the wave differences

Figure 10 shows the mean wind and wave parameters and the RMSDs of the SPT-interpolated parameters and the linearly interpolated parameters from 2005 to 2006. Figure 10a shows the mean wind speeds ($\overline{U_L}$), and Figure 10b shows the RMSDs of the wind speeds ($R_d(U_L, U_S)$). The position of the NDBC buoy (51.141° N, 179.119° W: the triangle in Figure 10) is close to the local maximum point of the wind speeds (Figure 10a) but is not close to the local maximum of the RMSD point of more than 0.8 ms^{-1}, which is near (40 N, 160° E) (Figure 10b). The maximum position of $R_d(U_L, U_S)$ in Figure 10b is at (38.25 N, 156.75° E). The contour lines of $\overline{U_L}$ are not dense and the magnitudes of the spatial gradient of $\overline{U_L}$ are not large in the area where $R_d(U_L, U_S)$ is large. The magnitudes of the spatial gradient of $\overline{U_L}$ in Figure 10a, except near the coast, are large from 150° E to 170° E and near 30° N.

Figure 10c shows the mean wave heights ($\overline{H_{sL}}$), and Figure 10d shows the RMSDs of the wave heights ($R_d(H_{sL}, H_{sS})$). The value of $R_d(H_{sL}, H_{sS})$ at the NDBC buoy location is approximately 0.07 m (the triangle in Figure 10), which is not large in Figure 10d. The spatial pattern of the wave heights in Figure 10c is similar to that of the wind speeds in Figure 10a.

Figure 10e shows the mean wave periods ($\overline{T_L}$), and Figure 10f shows the RMSDs of the wave periods ($R_d(T_L, T_S)$). The spatial pattern of the mean wave period is different from those of the wind speeds (Figure 10a) and the wave heights (Figure 10c). Conversely, the spatial pattern of the RMSDs of the wave periods ($R_d(T_L, T_S)$) is similar to those of the wind speeds (Figure 10b) and the wave heights (Figure 10d). The area where the RMSDs of the wind speeds between from the linear interpolation and from SPTIM is nearly the same to those of wave parameters. However, the large RMSD area is different from the area where either the values of the parameters or the magnitudes of the spatial gradients is not the large area of $R_d(U_L, U_S)$.

4. Discussion and conclusion

SPTIM can be applied to the interpolation of the surface winds even in the case where there are multiple cyclones and anticyclones that move in different directions and at different distances. The impact of SPTIM on wave prediction in the North Pacific area was investigated. The spatial resolution for the wave prediction was $0.75^\circ \times 0.75^\circ$. The comparison period was from 2005 to 2006. The data from six NBDC buoys and seven JMA drifting buoys were used.

The comparison between the NDBC-buoy-observed wave heights and periods and those predicted from the interpolated winds shows that the improvement in the correlation and RMSD due to SPTIM is small for the total dataset. In the case where the magnitude of the propagation vector $\mathbf{a}$ in Eq. (1) is small, the differences in the wind and wave parameters between those from the linear interpolation and those from SPTIM are small (Hisaki, 2016). However, the improvement is evident for larger differences in the wind and wave heights and periods between those from the linear interpolation and those from SPTIM. We showed that the improvements in the wave prediction are statistically significant at more than 95 % levels for most values of H_D and T_D.

The predicted wave directions at the position of buoy U, where the difference between the linearly interpolated winds and the SPT-interpolated winds is small, were compared with the observed wave directions. The prediction of the wave direction using SPTIM was not improved. This is because the direction of the SPT-interpolated wind was not improved compared to that of the linearly interpolated wind, while the speed of the SPT-interpolated wind was improved. If a (anti)cyclone exists, the reconstruction of the SPT-interpolated winds near the (anti)cyclone will be improved. However, if there are no (anti)cyclone near the area, the reconstruction of the SPT-interpolated winds near the (anti)cyclone will not be improved. In this case, the propagation vector **a** should be zero, which makes SPTIM identical to the linear interpolation. However, the propagation vector **a** may not be zero due to the spatial interpolation of the vector **a** on the grid points, as explained in Section 2.1. If there is a cyclone, the wind speed will be large around the area of the cyclone. The contribution of the improvement of the SPT-interpolated wind speed to the error statistics is large, while that of the SPT-interpolated wind direction is not very large. Consequently, the SPT-interpolated wind speed is improved even at buoy U. The method for the spatial interpolation of the propagation vector **a** should be improved in future studies.

The comparison between the JMA-buoy-observed wave heights and those predicted from the interpolated winds also shows the improvement in the correlation and the RMSD due to SPTIM with larger H_D. This improvement is evident, even though the number of comparisons with JMA buoys is much smaller than that with NDBC buoys. This is because the JMA buoys are drifting in the Kuroshio extension area, which is close to the storm track area. To the author's knowledge, this study demonstrates for the first time that the wave height and period prediction can only be improved by improving the time interpolation of the winds.

The area where the difference in the wind and wave parameters between those from the linear interpolation and those from SPTIM is large is in the storm track area of the North Pacific. The area where the wind speeds ($\overline{U_L}$) are the largest is not in the large area of $R_d(U_L, U_S)$. This is also true for the wave height and period. The area where the $R_d(U_L, U_S)$ are large is also different from the area where the magnitudes of the spatial gradients of the wind speeds are large. This is also true for the wave height and period. The differences in the wind and wave parameters between the linear interpolation and SPTIM are not very large over the two years. Therefore, the improvement in the wave prediction using SPTIM is small overall. However, often the wave prediction using SPTIM is improved at any locations.

The time resolution of the archived atmospheric reanalysis data will be higher in the future. However, SPTIM will still useful in this case. Not only the time resolution but also the spatial resolution will be finer in future archived atmospheric reanalysis datasets. The magnitudes of the propagation vector **a** in Eq. (1) in the horizontal coordinate normalized by the grid resolution are larger with finer spatial resolution.

SPTIM can also improve the spatial resolution. For example, consider the spatial interpolation from a 0.75° grid to a 0.25° grid. The 0.75° grid line overlaps the 0.25° grid line. A center of a cyclone at time t is detected on a 0.75° grid point, and the center of the cyclone at time $t + T$ is detected on another 0.75° grid point. The center of the cyclone at time $t{+}\alpha_t T$ ($0 < \alpha_t < 1$) is always on the 0.75° grid point in the case of the bilinear interpolation from a 0.75° grid to a 0.25° grid. However, the center position can be on a 0.25° grid point in the case of SPTIM. The impact of the spatial interpolation on the ocean modeling of surface waves or high frequency variability such as a near-inertial oscillations will be explored in future studies.

Acknowledgments

This study was financially supported by a Grant-in-Aid for Scientific Research (C-2) from the Ministry of Education, Culture, Sports, Science, and Technology of Japan (26420504). The GFD DENNOU Library (available online at http://www.gfd-dennou.org/arch/dcl/) was used for drawing the figures. Comments from editor and reviewer(s) were helpful in improving the manuscript.

References

Businger, S., Yildiz, S., Robinson, T.E., 2015. The impact of hurricane force wind fields on the North Pacific ocean environment. Weather and Forecasting 30, 742–753. doi:10.1175/WAF-D-14-00107.1.

Caires, S., Sterl, A., Bidlot, J., Graham, N., Swail, V., 2004. Intercomparison of different wind–wave reanalyses. Journal of Climate 17, 1893–1913. doi:10.1175/1520-0442(2004)017<1893:IODWR>2.0.CO;2.

Campos, R., Soares, C.G., 2016. Comparison of HIPOCAS and ERA wind and wave reanalyses in the North Atlantic Ocean. Ocean Engineering 112, 320–334. doi:10.1016/j.oceaneng.2015.12.028.

Chawla, A., Spindler, D.M., Tolman, H.L., 2013. Validation of a thirty year wave hindcast using the Climate Forecast System Reanalysis winds. Ocean Modelling 70, 189–206. doi:10.1016/j.ocemod.2012.07.005.

Cheung, K.F., Tang, L., Donnelly, J.P., Scileppi, E.M., Liu, K.B., Mao, X.Z., Houston, S.H., Murnane, R.J., 2007. Numerical modeling and field evidence of coastal overwash in southern New England from Hurricane Bob and implications for paleotempestology. Journal of Geophysical Research: Earth Surface 112. doi:10.1029/2006JF000612.

Chowdhury, P., Behera, M.R., 2017. Effect of long-term wave climate variability on longshore sediment transport along regional coastlines. Progress in Oceanography 156, 145–153. doi:10.1016/j.pocean.2017.06.001.

Cieślikiewicz, W., Graff, J., 1997. Sea state parameterisation using empirical orthogonal functions, in: Coastal Engineering 1996, pp. 703–716. doi:10.1061/9780784402429.056.

Cox, A.T., Swail, V.R., 2001. A global wave hindcast over the period 1958-1997- Validation and climate assessment. Journal of Geophysical Research: Oceans 106, 2313–2329. doi:10.1029/2001JC000301.

Doble, M.J., Bidlot, J.R., 2013. Wave buoy measurements at the Antarctic sea ice edge compared with an enhanced ECMWF WAM: Progress towards global waves-in-ice modelling. Ocean Modelling 70, 166–173. doi:10.1016/j.ocemod.2013.05.012.

Emery, W.J., Thomson, R.E., 1998. Data analysis methods in physical oceanography. Pergamon.

Graber, H.C., Jensen, R.E., Cardone, V.J., 1995. Sensitivity of wave model predictions on spatial and temporal resolution of the wind field. 4th intern, in: Workshop on Wave Hindcasting and Forecasting, pp. 16–20. URL: http://www.waveworkshop.org/4thWaves/4thWaves.pdf.

Hasselmann, S., Hasselmann, K., Allender, J., Barnett, T., 1985. Computations and parameterizations of the nonlinear energy transfer in a gravity-wave specturm. Part II: Parameterizations of the nonlinear energy transfer for application in wave models. Journal of Physical Oceanography 15, 1378–1391. doi:10.1175/1520-0485(1985)015<1378:CAPOTN>2.0.CO;2.

Hisaki, Y., 2011. Spectral interpolation of long-travelling predicted waves. Ocean Modelling 38, 217–229. doi:10.1016/j.ocemod.2011.03.003.

Hisaki, Y., 2016. Time interpolation of stationary and propagating surface disturbances for ocean modeling. Earth and Space Science 3, 346–361. doi:10.1002/2016EA000175.

Hisaki, Y., Naruke, T., 2003. Horizontal variability of near-inertial oscillations associated with the passage of a typhoon. Journal of Geophysical Research: Oceans 108. doi:10.1029/2002JC001683.

Hong, C.H., Yoon, J.H., 2003. A three-dimensional numerical simulation of Typhoon Holly in the northwestern Pacific ocean. Journal of Geophysical Research: Oceans 108. doi:10.1029/2002JC001563.

Hsu, S., Meindl, E.A., Gilhousen, D.B., 1994. Determining the power-law wind-profile exponent under near-neutral stability conditions at sea. Journal of Applied Meteorology 33, 757–765. doi:10.1175/1520-0450(1994)033<0757:DTPLWP>2.0.CO;2.

Janssen, P.A., 1991. Quasi-linear theory of wind-wave generation applied to wave forecasting. Journal of Physical Oceanography 21, 1631–1642. doi:10.1175/1520-0485(1991)021<1631:QLTOWW>2.0.CO;2.

Komen, G., Hasselmann, K., Hasselmann, K., 1984. On the existence of a fully developed wind-sea spectrum. Journal of Physical Oceanography 14, 1271–1285. doi:10.1175/1520-0485(1984)014<1271:OTEOAF>2.0.CO;2.

Nakamura, H., Sampe, T., Tanimoto, Y., Shimpo, A., 2004. Observed associations among storm tracks, jet streams and midlatitude oceanic fronts, in: Wang, C., Xie, S.P., Carton, J.A. (Eds.), Earth's Climate. American Geophysical Union. volume 147, pp. 329–345. doi:10.1029/147GM18.

Neu, U., Akperov, M.G., Bellenbaum, N., Benestad, R., Blender, R., Caballero, R., Cocozza, A., Dacre, H.F., Feng, Y., Fraedrich, K., et al., 2013. IMILAST: A community effort to intercompare extratropical cyclone detection and tracking algorithms. Bulletin of the American Meteorological Society 94, 529–547. doi:10.1175/BAMS-D-11-00154.1.

Phadke, A.C., Martino, C.D., Cheung, K.F., Houston, S.H., 2003. Modeling of tropical cyclone winds and waves for emergency management. Ocean Engineering 30, 553–578. doi:10.1016/S0029-8018(02)00033-1.

Pingree-Shippee, K.A., Shippee, N.J., Atkinson, D.E., 2016. Overview of Bering and Chukchi sea wave states for four severe storms following common synoptic tracks. Journal of Atmospheric and Oceanic Technology 33, 283–302. doi:10.1175/JTECH-D-15-0153.1.

Reguero, B., Menéndez, M., Méndez, F., Mínguez, R., Losada, I., 2012. A Global Ocean Wave (GOW) calibrated reanalysis from 1948 onwards. Coastal Engineering 65, 38–55. doi:10.1016/j.coastaleng.2012.03.003.

Sasaki, W., 2014. Changes in the North Pacific wave climate since the mid-1990s. Geophysical Research Letters 41, 7854–7860. doi:10.1002/2014GL061590.

Stopa, J.E., Cheung, K.F., 2014. Intercomparison of wind and wave data from the ECMWF Reanalysis Interim and the NCEP Climate Forecast System Reanalysis. Ocean Modelling 75, 65–83. doi:10.1016/j.ocemod.2013.12.006.

Trenberth, K.E., 1984. Some effects of finite sample size and persistence on meteorological statistics. Part II: Potential predictability. Monthly Weather Review 112, 2369–2379. doi:10.1175/1520-0493(1984)112<2359:SEOFSS>2.0.CO;2.

Van Vledder, G.P., Akpınar, A., 2015. Wave model predictions in the Black Sea: sensitivity to wind fields. Applied Ocean Research 53, 161–178. doi:10.1016/j.apor.2015.08.006.

WAMDI Group, et al., 1988. The WAM model-A third generation ocean wave prediction model. Journal of Physical Oceanography 18, 1775–1810. doi:10.1175/1520-0485(1988)018<1775:TWMTGO>2.0.CO;2.

Wang, X.L., Swail, V.R., 2001. Changes of extreme wave heights in Northern hemisphere oceans and related atmospheric circulation regimes. Journal of Climate 14, 2204–2221. doi:10.1175/1520-0442(2001)014<2204:COEWHI>2.0.CO;2.

Waseda, T., Sinchi, M., Kiyomatsu, K., Nishida, T., Takahashi, S., Asaumi, S., Kawai, Y., Tamura, H., Miyazawa, Y., 2014. Deep water observations of extreme waves with moored and free GPS buoys. Ocean Dynamics 64, 1269–1280. doi:10.1007/s10236-014-0751-4.

Wise Group, Cavaleri, L., Alves, J.H., Ardhuin, F., Babanin, A., Banner, M., Belibassakis, K., Benoit, M., Donelan, M., Groeneweg, J., Herbers, T., et al., 2007. Wave modelling–the state of the art. Progress in Oceanography 75, 603–674. doi:10.1016/j.pocean.2007.05.005.

Yamaguchi, M., Hatada, Y., 2002. 51-year wave hindcast and analysis of wave height climate trend of the Northwestern Pacific ocean, in: Proc. 7th Int. Workshop on Wave Hindcasting and Forecasting, U.S. Army Engineer Research and Development Center, Banff, AB, Canada. pp. 60–69. Available at http://www.waveworkshop.org /7thWaves/Papers/Yamaguchi_Hatada.pdf.

Zieger, S., Vinoth, J., Young, I., 2009. Joint calibration of multiplatform altimeter measurements of wind speed and wave height over the past 20 years. Journal of Atmospheric and Oceanic Technology 26, 2549–2564. doi:10.1175/2009JTECHA1303.1.

Zolina, O., Gulev, S.K., 2002. Improving the accuracy of mapping cyclone numbers and frequencies. Monthly Weather Review 130, 748–759. doi:10.1175/1520-0493(2002)130<0748:ITAOMC>2.0.CO;2.

Table 1: Summary of NDBC buoys for comparison. The values from the second line to the seventh line (from buoy P to U) are those for the winds, wave heights, and periods. The values of the bottom (eighth) line (buoy U) are those for the wave directions. The locations of the buoys are shown in Figure 1a. N_{wn} indicates the number of wind data for comparison, and N_{wv} indicates the number of wave data for comparison.

Buoy	Buoy ID	Position	Period (hour/day/month/year)	N_{wn}	N_{wv}
P	46071	(51.14° N, 179.12° E)	0/1/1/2005-23/31/12/2006	16469	15761
Q	46072	(51.66° N, 172.06° W)	0/1/1/2005-10/14/10/2006	8472	15386
R	46073	(55.03° N, 172.00° W)	21/13/5/2005-23/31/12/2006	14194	14059
S	46075	(53.91° N, 160.82° W)	0/1/1/2006-23/31/5/2006	7204	9419
T	46035	(57.03° N, 177.74° W)	0/1/1/2005-23/31/12/2006	13130	17364
U	51001	(24.417° N, 162.10° W)	0/1/1/2005-23/31/12/2006	17471	17329
U	51001	(24.417° N, 162.10° W)	0/1/6/2005-23/31/12/2006		13726

Table 2: Summary of the JMA drifting buoy specifications. The JMA buoys are shown in Figure 1b. N_{wv} indicates the number of wave heights for comparison.

Buoy	Initial Position	End Position	Period (hour/day/month/year)	N_{wv}
A	(31.85° N,145.01° E)	(31.28° N,147.32° E)	06/13/02/2005-15/11/03/2005	212
B	(41.26° N,145.06° E)	(40.18° N,145.02° E)	06/02/05/2005-03/09/05/2005	56
C	(39.12° N,145.00° E)	(41.15° N,156.05° E)	06/06/07/2005-00/28/09/2005	667
D	(35.36° N,145.11° E)	(31.05° N,168.73° E)	03/18/08/2005-12/06/12/2005	882
E	(35.79° N,145.02° E)	(35.31° N,168.13° E)	12/05/06/2006-09/29/11/2006	1365
F	(34.43° N,145.02° E)	(36.53° N,154.55° E)	00/29/08/2006-21/28/10/2006	483
G	(40.80° N,145.03° E)	(38.33° N,148.66° E)	18/12/11/2006-21/31/12/2006	290

Table 3: Comparisons of the predicted wind speeds with the wind speeds from the NDBC buoys. The locations of the NDBC buoys are shown in Figure 1a.

Wind speed, unit: m/s for the RMSD and mean values							
Buoy	$r_c(U_B, U_L)$	$r_c(U_B, U_S)$	$R_d(U_B, U_L)$	$R_d(U_B, U_S)$	$\overline{U_B}$	$\overline{U_L}$	$\overline{U_S}$
P	0.903	0.904	1.846	1.834	8.357	8.459	8.489
Q	0.913	0.915	1.659	1.633	8.669	8.468	8.501
R	0.952	0.954	2.077	2.039	9.841	8.441	8.466
S	0.924	0.926	1.620	1.604	8.736	8.191	8.194
T	0.951	0.952	2.260	2.231	10.654	9.064	9.089
U	0.849	0.849	1.737	1.741	7.534	6.638	6.635

Table 4: Comparisons of the predicted wave heights and periods to those from the NDBC buoys. The locations of the NDBC buoys are shown in Figure 1a.

Wave height, unit: m for the RMSD and mean values							
Buoy	$r_c(H_{sB}, H_{sL})$	$r_c(H_{sB}, H_{sS})$	$R_d(H_{sB}, H_{sL})$	$R_d(H_{sB}, H_{sS})$	$\overline{H_{sB}}$	$\overline{H_{sL}}$	$\overline{H_{sS}}$
P	0.859	0.864	0.818	0.805	2.806	2.869	2.884
Q	0.918	0.920	0.637	0.624	2.930	2.754	2.771
R	0.947	0.948	0.554	0.557	2.402	2.682	2.697
S	0.882	0.886	0.627	0.618	2.569	2.618	2.632
T	0.949	0.951	0.503	0.497	2.610	2.681	2.691
U	0.824	0.826	0.642	0.638	2.369	1.930	1.933
All	0.893	0.895	0.638	0.631	2.616	2.575	2.586
Wave period, unit: s for the RMSD and mean values							
Buoy	$r_c(T_B, T_L)$	$r_c(T_B, T_S)$	$R_d(T_B, T_L)$	$R_d(T_B, T_S)$	$\overline{T_B}$	$\overline{T_L}$	$\overline{T_S}$
P	0.738	0.743	1.333	1.322	7.133	6.289	6.298
Q	0.802	0.805	1.291	1.276	7.142	6.238	6.251
R	0.766	0.765	0.972	0.966	6.626	6.118	6.130
S	0.740	0.744	1.121	1.104	6.709	6.137	6.158
T	0.791	0.792	1.032	1.025	6.622	6.045	6.053
U	0.807	0.809	1.805	1.792	7.343	5.824	5.835
All	0.747	0.749	1.312	1.301	6.951	6.099	6.112

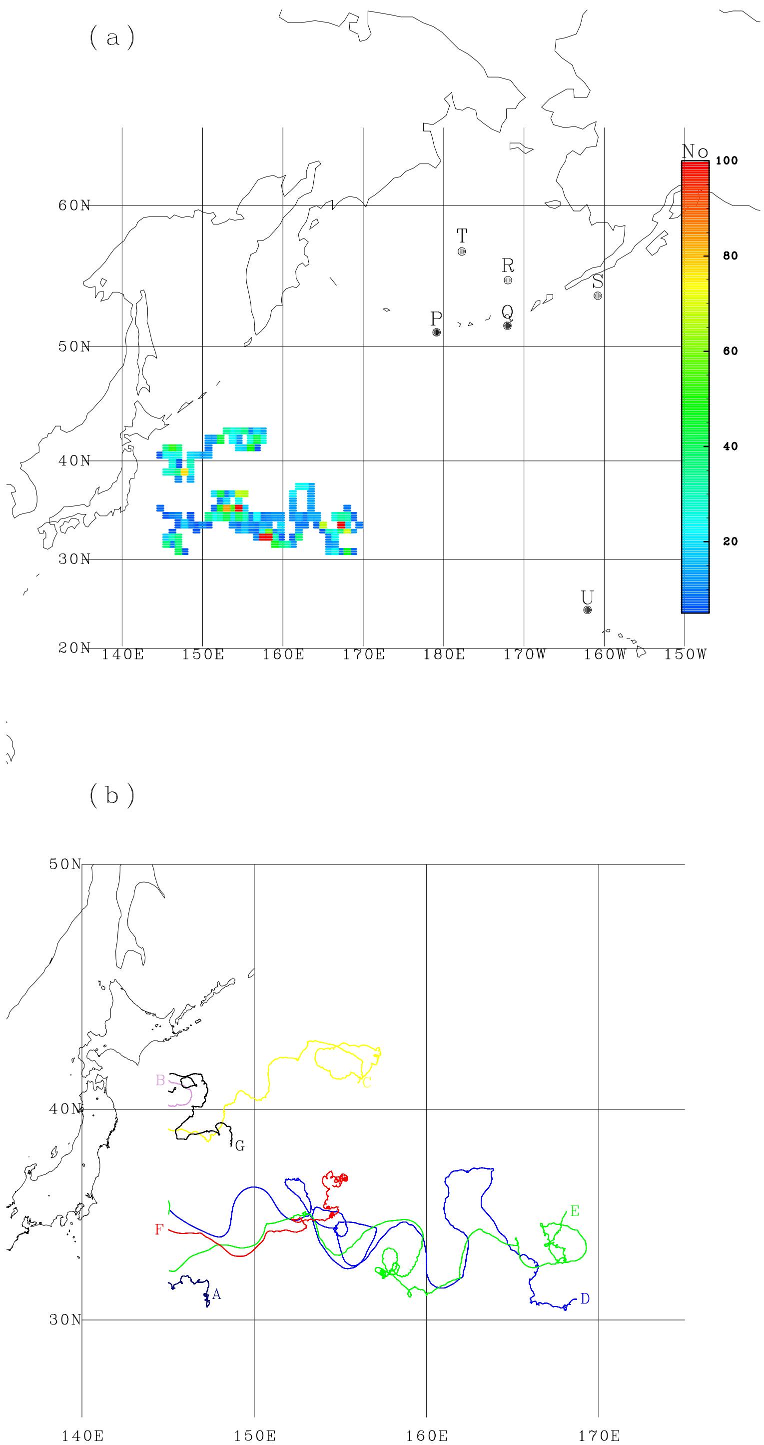

Figure 1: (a) NDBC buoy locations and the number of data points for the JMA drifting buoys in the 0.75° bin during the analysis period and (b) trajectories of the JMA drifting buoys used for the analysis.

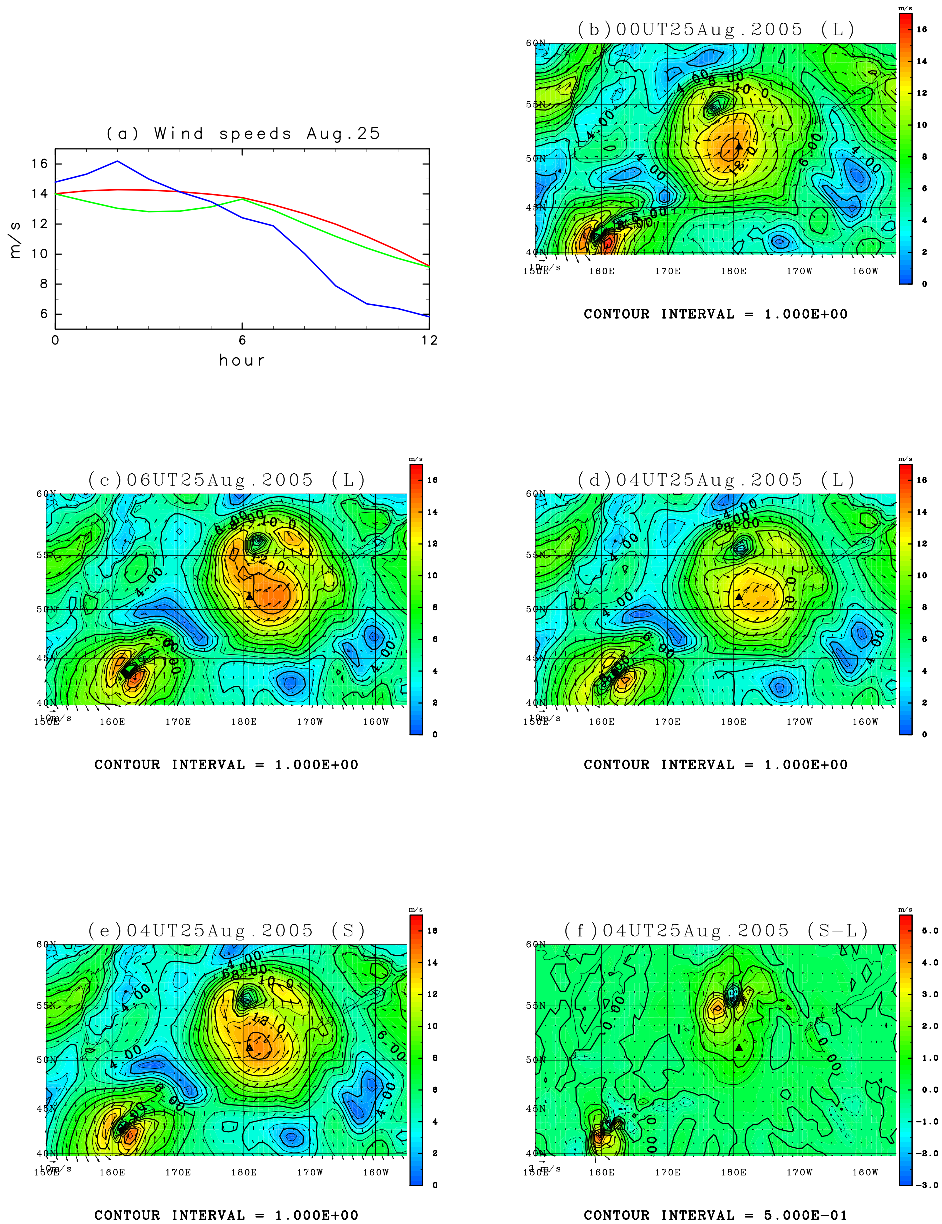

Figure 2: (a) Time series of the buoy-observed wind speed (U_B: blue), the linearly interpolated wind speeds (U_L: green), and the SPT-interpolated wind speeds (U_S: red) at the NDBC buoy (P) location from 0 UTC to 12 UTC on August 25, 2005. (b) Wind speeds and vectors at 0 UTC on August 25, 2005. (c) Same as panel (b) but at 6 UTC. (d) Linearly interpolated wind speeds (U_L) and vectors ($\mathbf{U}_L$) at 4 UTC on August 25, 2005. (e) Same as panel (d) but for U_S and $\mathbf{U}_S$. (f) Differences in the speeds and vectors between the SPT-interpolated and linearly interpolated winds ($U_S - U_L$ and $\mathbf{U}_S - \mathbf{U}_L$).

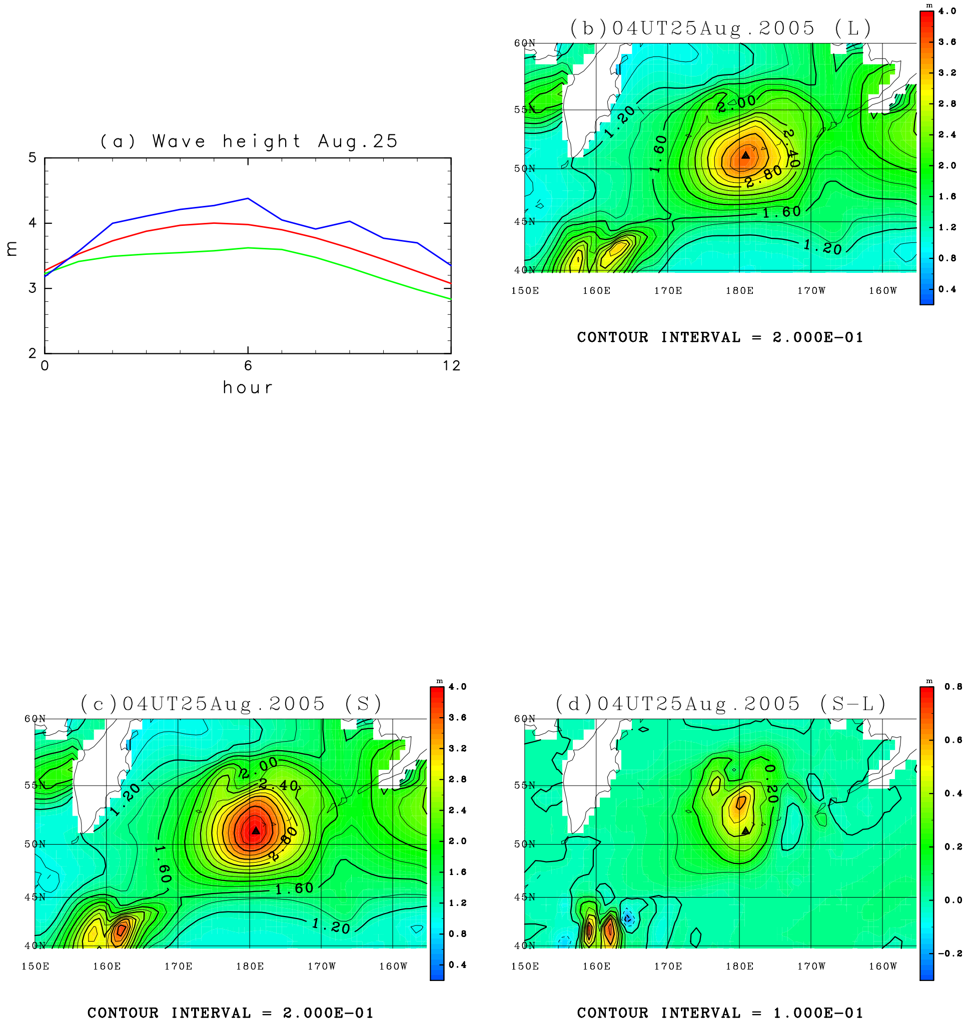

Figure 3: (a) Time series of the buoy-observed wave heights (H_{sB}: blue), the predicted wave heights from the linearly interpolated winds (H_{sL}: green), and the SPT-interpolated winds (H_{sS}: red) at the NDBC buoy location from 0 UTC to 12 UTC on August 25, 2005. (b) Contours are the same as those in Figure 2d but for the predicted wave heights from the linearly interpolated winds (H_{sL} at 4 UTC on August 25, 2005). (c) Same as panel (b) but from the SPT-interpolated winds (H_{sS} at 4 UTC on August 25, 2005). (d) Differences in the predicted wave heights between the SPT-interpolated and linearly interpolated winds ($H_{sS}-H_{sL}$) at 4 UTC on August 25, 2005.

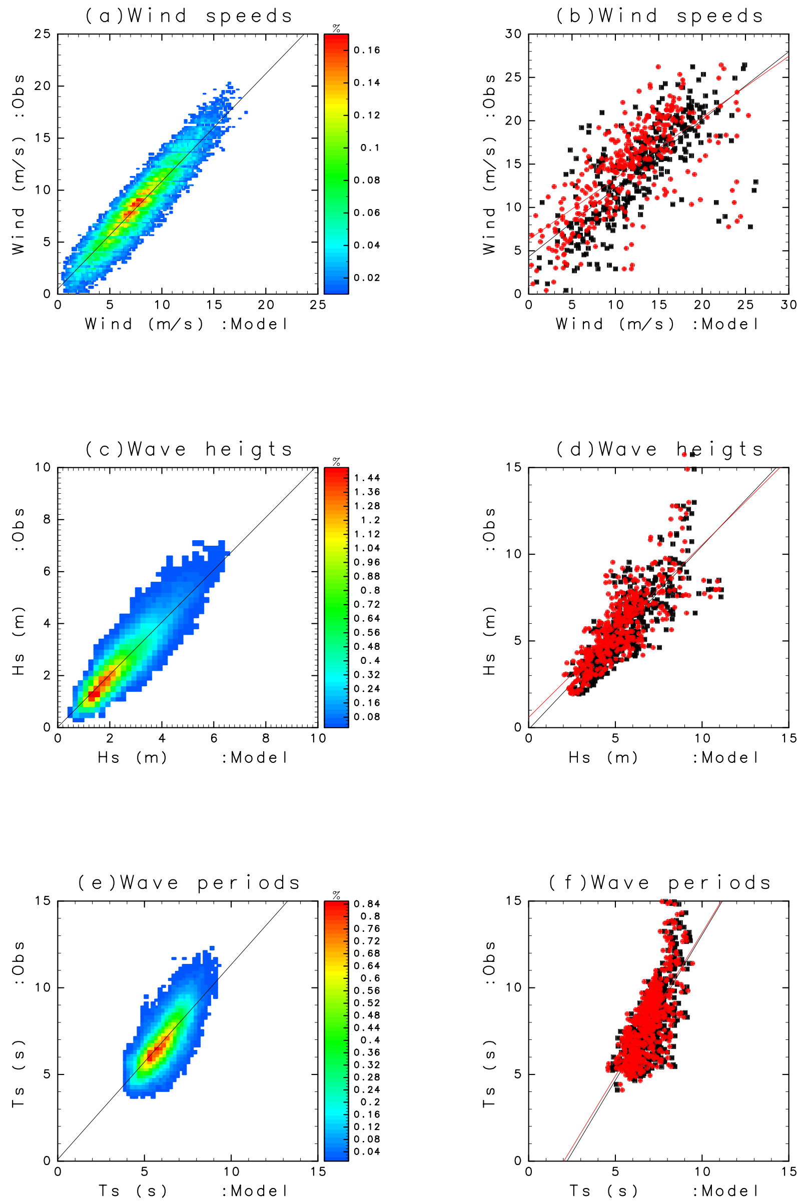

Figure 4: (a) Scatter plot of the linearly interpolated wind speeds (U_L) versus the buoy-observed wind speeds (U_B) for the data in the 0.2 ms^{-1} bin. The line indicates the linear regression. (b) Scatter plot of the buoy-observed wind speeds (U_B) versus the SPT-interpolated wind speeds (U_S: black) and the linearly interpolated wind speeds (U_L: red) in the case of $|U_S - U_L| > U_D$ and $U_D = 1.6$ ms^{-1}. The black line indicates the linear regression for U_B and U_S. The red line indicates the linear regression for U_B and U_L. (c) Same as panel (a) but for the wave heights and the 0.2 m bins, (d) same as panel (b) but for the wave heights and H_D= 0.3 m, (e) same as panel (a) but for the wave periods and the 0.2 s bins, and (f) same as panel (b) but for the wave periods and T_D= 0.2 s.

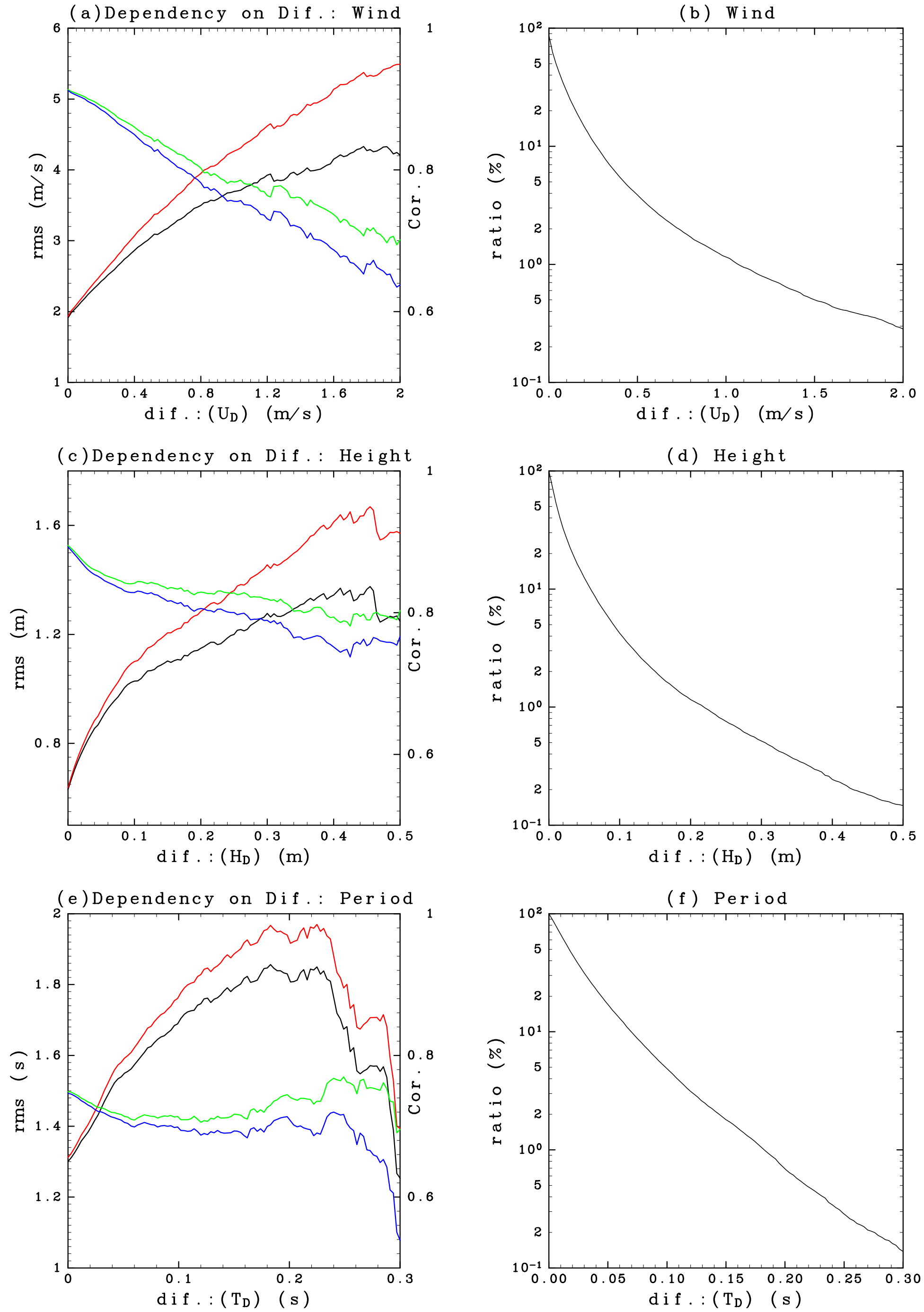

Figure 5: (a) RMS differences of the wind speeds $R_d(U_B, U_L)$ (red and left vertical axis) and $R_d(U_B, U_S)$ (black and left vertical axis), and the correlation of the wind speeds $r_c(U_B, U_L)$ (blue and right vertical axis) and $r_c(U_B, U_S)$ (green and right vertical axis) versus U_D (horizontal axis) for the case of $|U_S - U_L| > U_D$. (b) Percentage of the number of data points versus U_D for $|U_S - U_L| > U_D$. (c) Same as panel (a) but for the wave height, (d) same as panel (b) but for the wave height, (e) same as panel (a) but for the wave period, and (f) same as panel (b) but for the wave period.

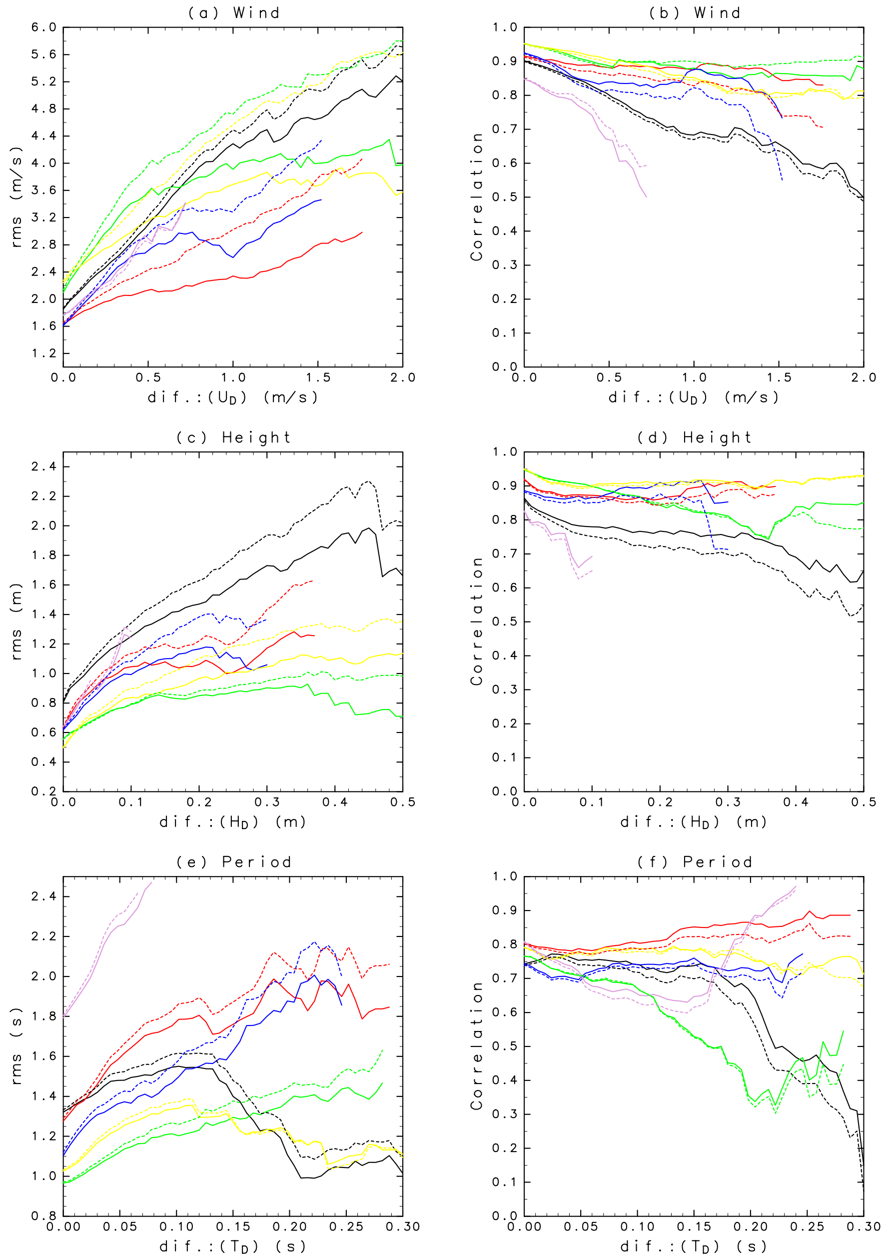

Figure 6: (a) The dashed lines indicate the RMS differences of the wind speeds $R_d(U_B, U_L)$ versus U_D (horizontal axis) in the case of $|U_S - U_L| > U_D$ for each NDBC buoy. The solid lines indicate the RMS differences of the wind speeds $R_d(U_B, U_S)$ (black: P, red: Q, green: R, blue: S, yellow: T, and purple: U). The locations of the NDBC buoys are shown in Figure 1a. (b) Same as panel (a) but for the correlations ($r_c(U_B, U_L)$ and $r_c(U_B, U_S)$). (c) Same as panel (a) but for the predicted wave heights ($R_d(H_{sB}, H_{sL})$ and $R_d(H_{sB}, H_{sS})$). (d) Same as panel (b) but for predicted wave heights ($r_c(H_{sB}, H_{sL})$ and $r_c(H_{sB}, H_{sS})$). (e) Same as panel (a) but for the predicted wave periods ($R_d(T_B, T_L)$ and $R_d(T_{sB}, T_S)$). (f) Same as panel (b) but for the predicted wave periods ($r_c(T_B, T_L)$ and $r_c(T_B, T_S)$).

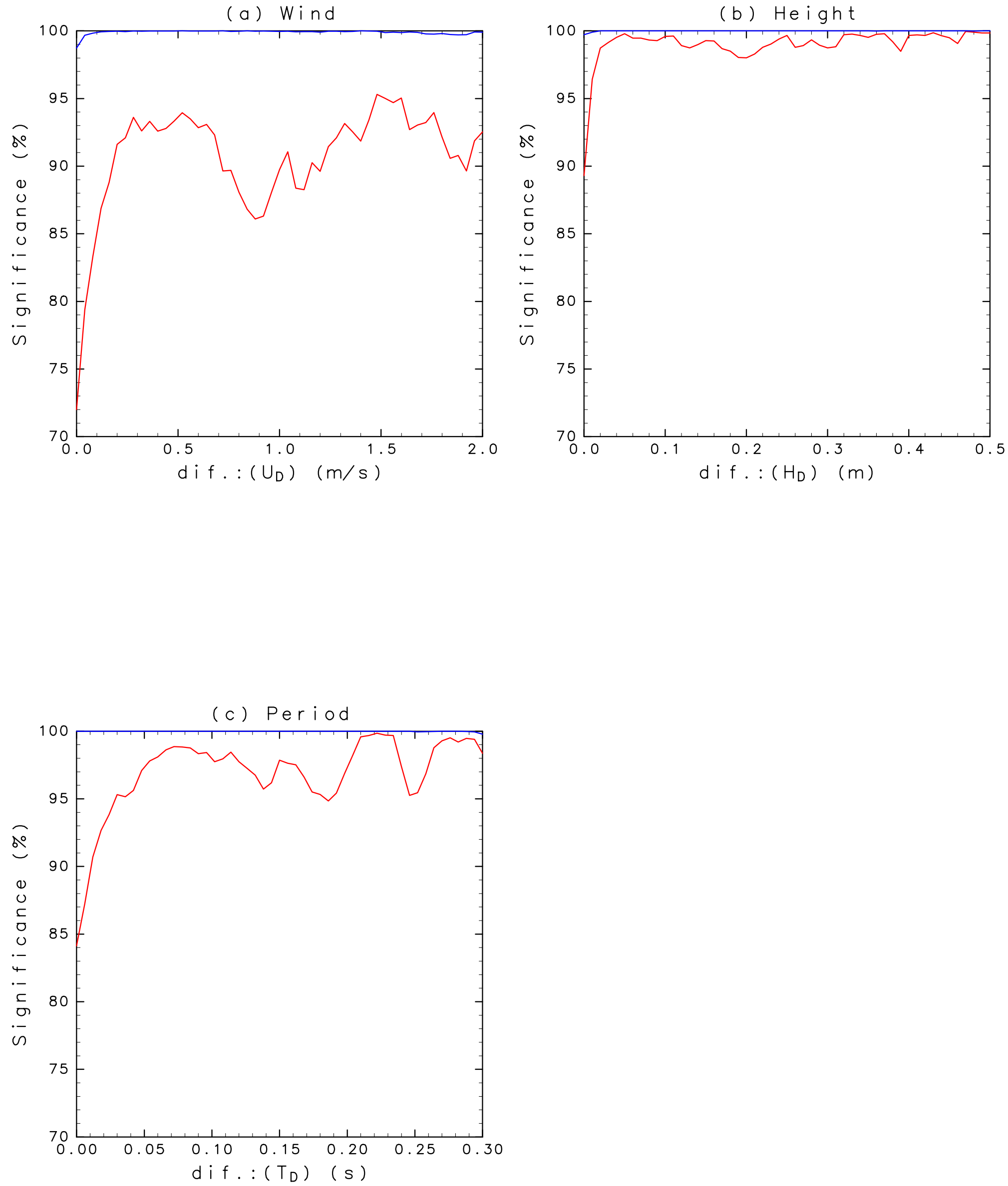

Figure 7: Significance level of the wave prediction improvement as a function of the difference between the linearly interpolated wave parameters and the SPT-interpolated wave parameters. (a) Significance level of the improvement of the wind speed correlation (red) and the RMSD of the wind speeds (blue). (b) Same as panel (a) but for the wave heights, and (c) same as panel (a) but for the wave periods.

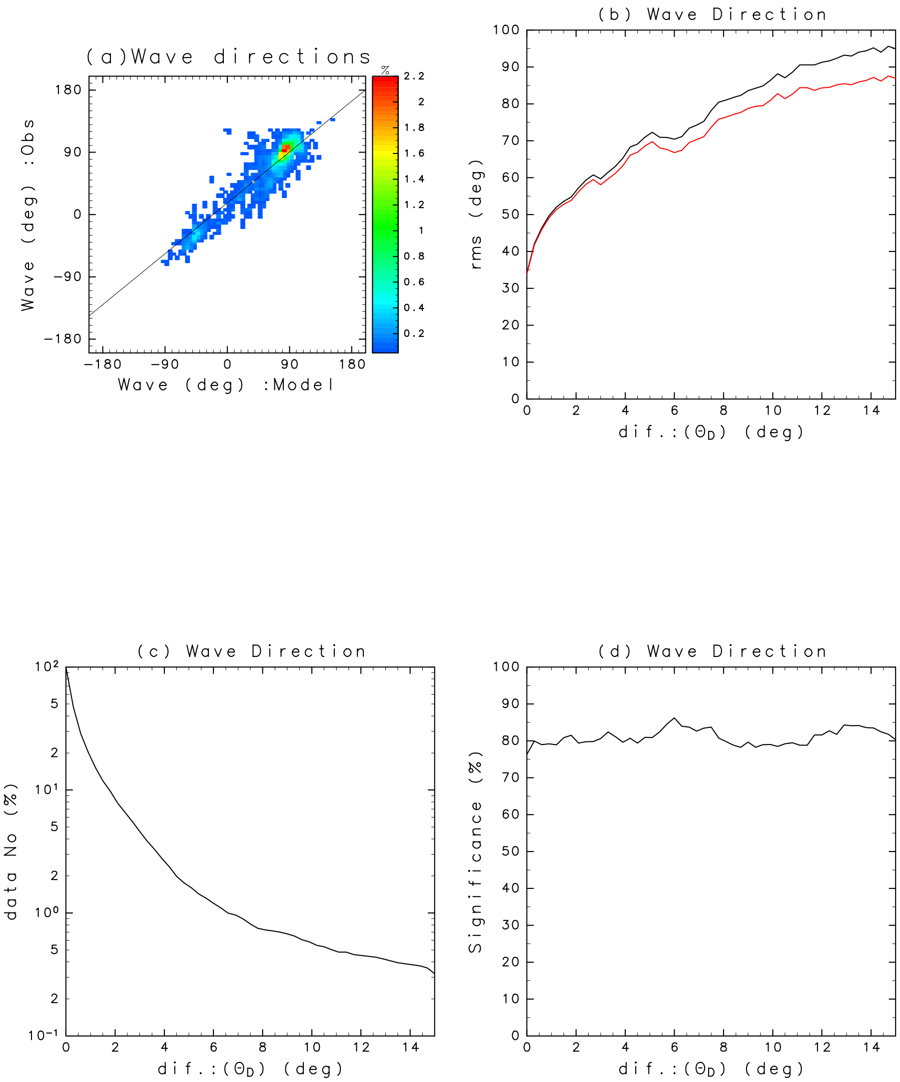

Figure 8: (a) Scatter density plot of the wave directions from the linearly interpolated winds (θ_{vL}) versus those observed by buoy U (θ_{vB}) in 5°×5° bins. (b) RMSDs between the predicted wave directions and the buoy-observed wave directions as a function of θ_D satisfying $|\theta_{vS} - \theta_{vL}| > \theta_D$ (black: $R_d(\theta_{vS}, \theta_{vB})$ and red: $R_d(\theta_{vL}, \theta_{vB})$). (c) Ratio of the number of wave direction data to the total number of wave direction data as a function of θ_D. (d) Probabilities of $R_d(\theta_{vS}, \theta_{vB}) < R_d(\theta_{vL}, \theta_{vB})$ as a function of θ_D estimated using the bootstrap method.

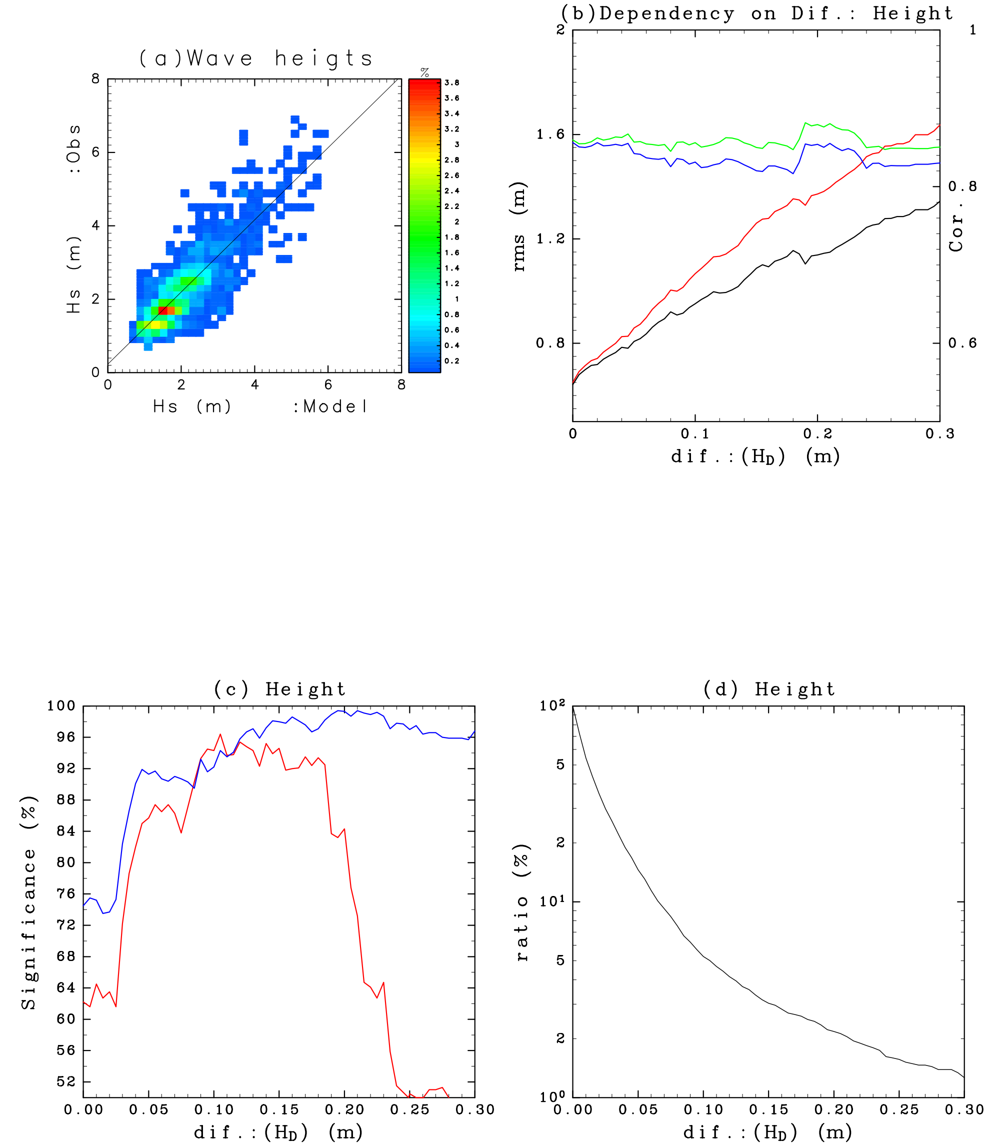

Figure 9: Comparisons of the wave heights predicted with the JMA drifting buoys. (a) Same as Figure 4c but with the JMA drifting buoys. (b) RMS differences of the wave heights $R_d(H_{sB}, H_{sL})$ (red, left vertical axis) and $R_d(H_{sB}, H_{sS})$ (black, left vertical axis), and the correlation of the wind speeds $r_c(H_{sB}, H_{sL})$ (blue, right vertical axis) and $r_c(H_{sB}, H_{sS})$ (green, right vertical axis) versus H_D (horizontal axis) in the case of $|H_{sS} - H_{sL}| > H_D$ for the JMA drifting buoys. (c) Same as Figure 7b but for the JMA drifting buoys. (d) Same as Figure 5d but for the JMA drifting buoys.

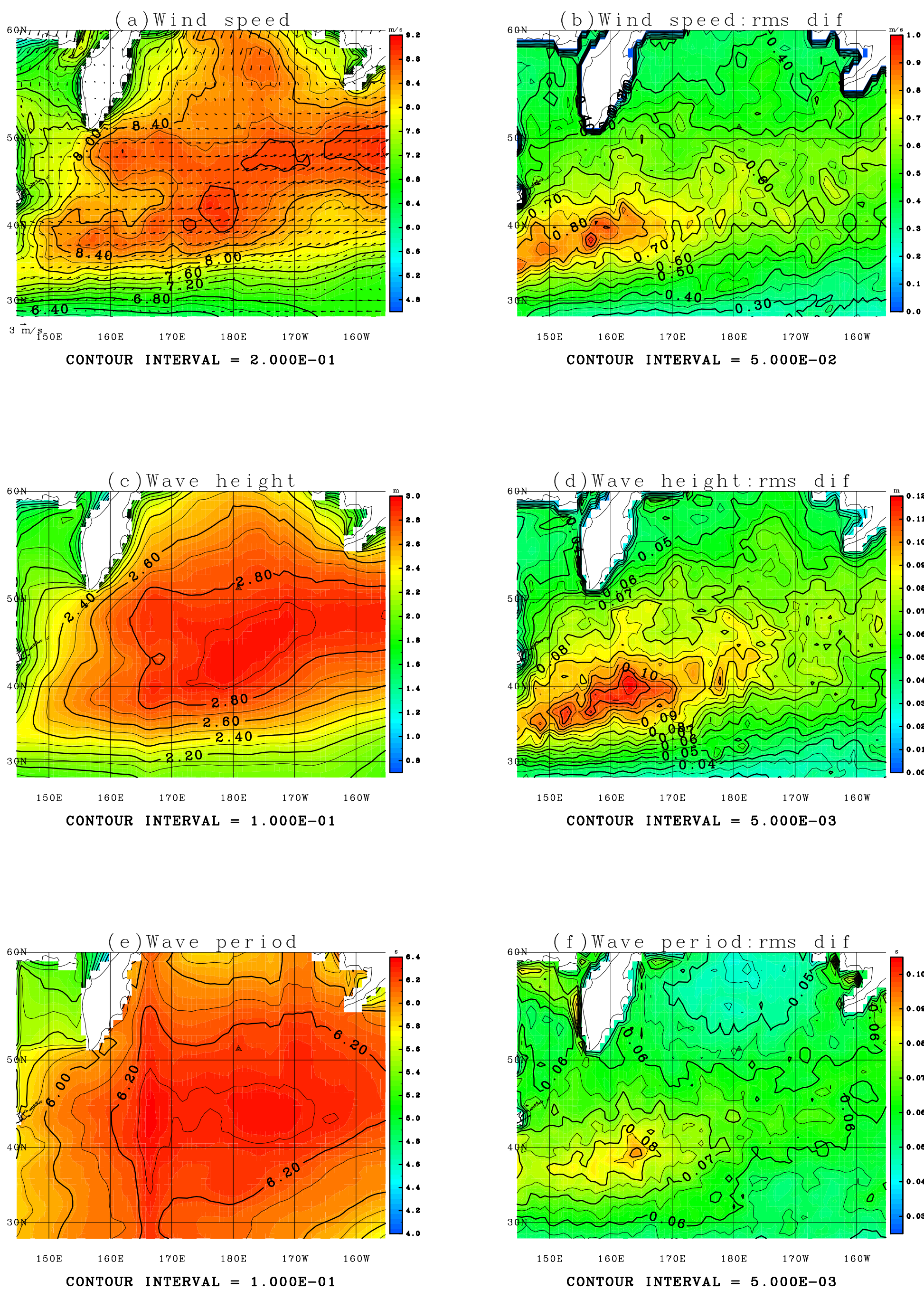

Figure 10: (a) Mean wind speed ($\overline{U_L}$) on the sea and the vectors ($\overline{\mathbf{U}_L}$) from the linear interpolation from 2005 to 2006. (b) RMS difference between U_L and U_S ($R_d(U_L, U_S)$) from 2005 to 2006. (c) Mean wave height ($\overline{H_{sL}}$) from 2005 to 2006. (d) Same as panel (b) but for the wave height ($R_d(H_{sL}, H_{sS})$). (e) Same as panel (c) but for the wave period ($\overline{T_L}$). (f) Same as panel (b) but for the wave period ($R_d(T_L, T_S)$).